Environmental Earth Sciences (2025) 84:318
https://doi.org/10.1007/s12665-025-12318-w

ORIGINAL ARTICLE

Evaluating contaminant pathways in an altered vadose zone: a multidisciplinary approach in open-pit quarry environments

Yazeed van Wyk[1,2] · Jacques Bodin[3] · Kai Witthüser[4] · Eunice Ubomba-Jaswa[2] · Matthys Alois Dippenaar[1] · Mike Butler[5]

Received: 16 December 2024 / Accepted: 9 May 2025 / Published online: 26 May 2025

Abstract

The closure of mining operations presents significant environmental challenges for groundwater protection and sustainable closure planning. Fractured and altered aquifers, which supply drinking water to nearly half the world's population, are vulnerable to disruptions caused by mining. This study investigates groundwater flow and contaminant dynamics in an altered vadose zone and fractured rock environment at a quarry situated 20 km east of Pretoria, South Africa. The primary objective is to develop effective monitoring strategies for groundwater protection post-mine closure. The heterogeneous geological structures, including a network of fractures and a diabase sill, generate distinct water types and flow dynamics, with active groundwater circulation despite seasonal fluctuations. Field investigations and tracer analyses revealed seasonal variations in transport parameters. Blasting activities modified fracture characteristics, creating new pathways and increasing connectivity between fracture networks, complicating contaminant migration. Tracer tests analysed with the MDMi and MDP-2RNE analytical models identified variations in Péclet numbers and mean transit times, with higher transport velocities and lower retardation factors during the wet season. The MDMi model was more sensitive to fracture connectivity changes, while the MDP-2RNE model highlighted seasonal differences in flow velocities and dispersion. These findings highlight the challenges of parameterisation and the necessity for seasonal calibration in modelling contaminant transport. A conceptual site model (CSM) illustrates how mining has transformed groundwater flow patterns and contaminant transport mechanisms, providing critical insights into sustainable groundwater management and mine closure planning. This research highlights the importance of targeted monitoring strategies to protect groundwater in altered vadose zone environments post-mine closure.

Highlights

- Integrated use of environmental and artificial tracers in vadose zone studies.
- Tracer tests revealed seasonal variations in velocities and fracture connectivity.
- Blasting modified fracture characteristics, creating new groundwater pathways.
- Conceptual site model developed to assess flow in an altered vadose zone.
- Seasonal calibration and parameterisation, a must for post-mine closure settings.

Keywords Altered vadose zone · Groundwater · Preferential flow · Artificial tracers · Environmental tracers · Stable isotopes

✉ Matthys Alois Dippenaar
matthys.dippenaar@up.ac.za; madippenaar@gmail.com

[1] Department of Geology, University of Pretoria, Hatfield Campus, Pretoria, South Africa

[2] Water Research Commission, Private Bag X03, Gezina, Pretoria 0031, South Africa

[3] Université de Poitiers, CNRS, UMR 7285 IC2MP, CEDEX, 40 Avenue du Recteur Pineau, Poitiers 86022, France

[4] Institute for Groundwater Studies, Faculty of Agricultural and Natural Sciences, University of the Free State, Bloemfontein, Free State 9301, South Africa

[5] iThemba Labs, Private Bag 11, Wits, Johannesburg, Gauteng 2050, South Africa

Introduction

The global demand for freshwater is escalating rapidly due to population growth, expanding agriculture, industrial development, and increasing urbanisation (McDonald et al. 2014năduc et al. 2022). These pressures are particularly acute in semi-arid regions like South Africa, where water scarcity is a persistent challenge. Additionally, climate change is intensifying these stresses by altering hydrological cycles and reshaping precipitation patterns, leading to more frequent and severe droughts, floods, and unpredictable groundwater recharge rates (Döll et al. 2015). This exacerbates the depletion of freshwater resources, making surface water supplies increasingly unreliable. Groundwater provides a more resilient source of water, serving as a buffer against surface water variability and offering a critical reserve during drought periods (Cuthbert et al. 2019).

Groundwater is estimated to account for approximately 30% of the world's freshwater, with around 70% of this used for agricultural irrigation (Ingrao et al. 2023). In regions with extensive open-pit mining, such as North America, Australia, and parts of Asia, groundwater is heavily relied upon both for operational needs and as a buffer against fluctuating surface water availability (Northey et al. 2016; Cook et al. 2017). Groundwater use in mining, including for dust suppression and ore processing, accounts for 7–12% of total withdrawals in these regions (Luo et al. 2022).

South Africa, as part of sub-Saharan Africa, faces significant challenges as surface water resources are under pressure to meet national water demand due to changing rainfall patterns and increased evapotranspiration (Baudoin et al. 2017; Mahlalela et al. 2020). Groundwater, therefore, plays an increasingly important role, supplementing insufficient surface water supplies, especially in agriculture. Despite its importance, groundwater is often not optimally or sustainably utilised (Braune and Xu 2010). Currently, groundwater accounts for only 13% of the nation's total water supply. However, it serves as a vital resource for approximately 56% of the population, or over 34 million people, across 23 746 settlements, particularly in rural and urban areas (Kotzé et al. 2019). Groundwater sustains livelihoods for 74% of rural inhabitants and 66% of urban residents, making it crucial for both development and survival. It is predominantly used for agricultural irrigation, accounting for around 64% of total groundwater abstraction, while approximately 8% is utilised for mining and domestic purposes (Knüppe 2011).

Mining activities, especially open-pit mining, represent an additional stressor on groundwater resources. Both underground and open-pit mining have been shown to impact water quality and disrupt local flow regimes, particularly within the vadose zone. In such environments, mining activities can alter the vadose zone by changing its structure and permeability, thereby affecting contaminant transport pathways and groundwater recharge. This altered vadose zone becomes a critical area of concern for contaminant migration, influencing the way in which pollutants move through the subsurface. A well-documented issue in both types of mining is acid mine drainage (AMD), where the oxidation of sulphide minerals generates acidic water rich in heavy metals and sulphates (Candeias et al. 2018; Fernando et al. 2018). This contaminated water can infiltrate nearby aquifers or be discharged into surface water systems, severely degrading water quality (Younger and Wolkersdorfer 2004).

Open-pit mining, in particular, often results in large voids that alter groundwater flow paths, leading to dewatering of surrounding areas or, in some cases, the formation of pit lakes that act as sinks for contaminated water (Bozan et al. 2022). Meanwhile, underground mining can cause subsidence and fracturing, creating new pathways for water movement, increasing the risk of contamination spreading into adjacent aquifers or surface water bodies (Zeng et al. 2018). Both types of mining also contribute to increased turbidity, sedimentation, and altered chemical profiles of nearby water bodies due to the mobilisation of fine particles and pollutants during excavation and dewatering processes.

Dewatering activities can lower water tables, reduce baseflow contributions to streams and rivers, and disrupt ecosystems dependent on consistent water availability (Nordstrom et al. 2015). Conversely, the cessation of mining operations may lead to the flooding of underground workings or the filling of open pits, reversing flow directions (only seasonally for pit lakes) and creating new hydrogeological conditions, including the risk of contaminated water re-entering the environment (Vervoort and Declercq 2018). These impacts, documented in both humid and arid environments, emphasise the need for comprehensive water management strategies in mining regions worldwide.

This study focuses on advancing a more accurate simulation of contaminant transport in open-pit quarry environments using an integrated approach. This includes tracer analysis, environmental isotopes, tritium, water quality assessments, and analytical modelling. The analytical modelling component in particular relies on estimating flow paths, residence times, and velocities, with assumptions made regarding fracture connectivity, flow heterogeneity, and the impact of seasonal variations. These estimations improve the predictive capacity for contaminant movement, allowing for more tailored groundwater management strategies (Van Wyk et al. 2024). Incorporating these advanced methodologies into broader water management frameworks enhances groundwater vulnerability assessments and promotes resilience against both anthropogenic pressures and climate change. More specifically, the analytical modelling

conducted in this study involve detailed estimations and assumptions regarding flow dynamics and contaminant behaviour. In doing so, this research supports the broader objective of ensuring that groundwater remains a sustainable and resilient resource amidst mounting environmental and societal pressures.

Study area

The study site is an open-pit quartzite and sandstone quarry located approximately 20 km east of Pretoria, South Africa. The quarry spans an area of 84 ha, encompassing Portions 46, 47, and 180, of the Farm Zwavelpoort 373 JR. Mining operations at this site commenced in the 1960s and continued until its closure in November 2023, following decades of aggregate extraction. The quarry is situated on the northeastern slope of the Bronberg Ridge with the plant facilities positioned on flatter terrain. The site features steep topography typical of hard-rock open-pit quarries, which are often associated with large landscape modifications and altered hydrogeological conditions (Li et al. 2016; Ran et al. 2018).

A major slope failure occurred in March 2009 on the southwestern slope of the quarry. The failure was attributed to water infiltration acting on a diabase sill which caused the rock mass to slide. Investigations revealed that continued failure along the length of the diabase sill was likely until all material above it lost stability. This failure remains a key geological and hydrogeological feature of the quarry, illustrating the interplay between groundwater infiltration and slope stability (Bezie et al. 2024). The closure of the quarry presents a unique opportunity to study the long-term impacts of mining on groundwater systems, slope stability, and landscape evolution. A locality map indicating detailed location and topographical features of the study area and a photograph illustrating the slope failure are given in Fig. 1.

The local geology is dominated by the Daspoort Formation quartzites, which are underpinned by the shales and hornfels of the Silverton Formation. The ore deposit consists of a competent rock mass quartzite deposit intruded by several sub-vertical dipping diabase dykes and sills of Bushveld age. The general dip (10º – 15º) of the bedding planes is to the northeast, and a prominent sub-vertical joint set strikes northwest. Additionally, two faults are present to the northwest of the existing pit, while another fault trends northeast in the western section of the mine, as shown on the geological map (1:250 000-scale 2528 Pretoria Geological Sheet) (Fig. 2).

Groundwater seepage is evident along the weathered diabase-quartzite contacts with runoff naturally flowing towards the quarry pit after rainfall (Fig. 3). The depositional and structural history of the area, including the influence of diabase intrusions and faulting, plays a crucial role in both the hydrology and geotechnical stability of the quarry.

Climate and topography

The quarry site is located within quaternary catchment A23A (Fig. S1) that is part of the Crocodile West and Marico Water Management Area (WMA) in the Gauteng Province. The area contains several drainage lines, seepage zones, and an artificial dam, all of which drain eastward into the Pienaars River; the quarry site is located approximately 6 km from this river. Some drainage lines flow into the quarry pit where water is used for dust suppression and processing. The site characteristics of the quaternary catchment are outlined in Table 1.

The quarry is situated along the Bronberg Ridge, with steep gradients at the southwestern edge (Fig. 4).

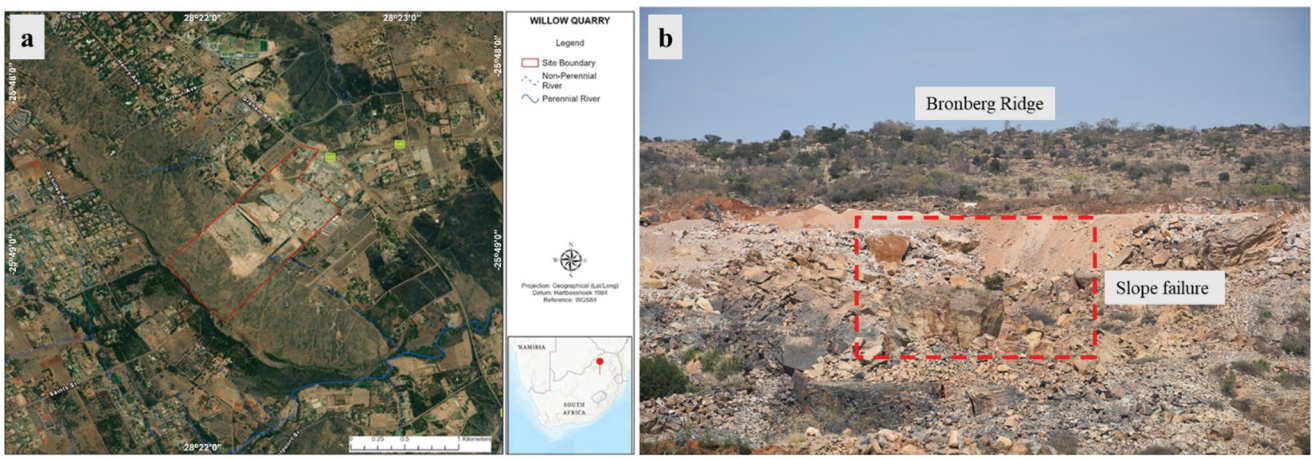

Fig. 1 (**a**) Locality map of the open-pit quarry on the Bronberg Ridge, east of Pretoria, South Africa; and (**b**) photograph of the March 2009 slope failure on the southwestern slope, caused by water infiltration along a diabase sill (photograph by van Wyk 2023)

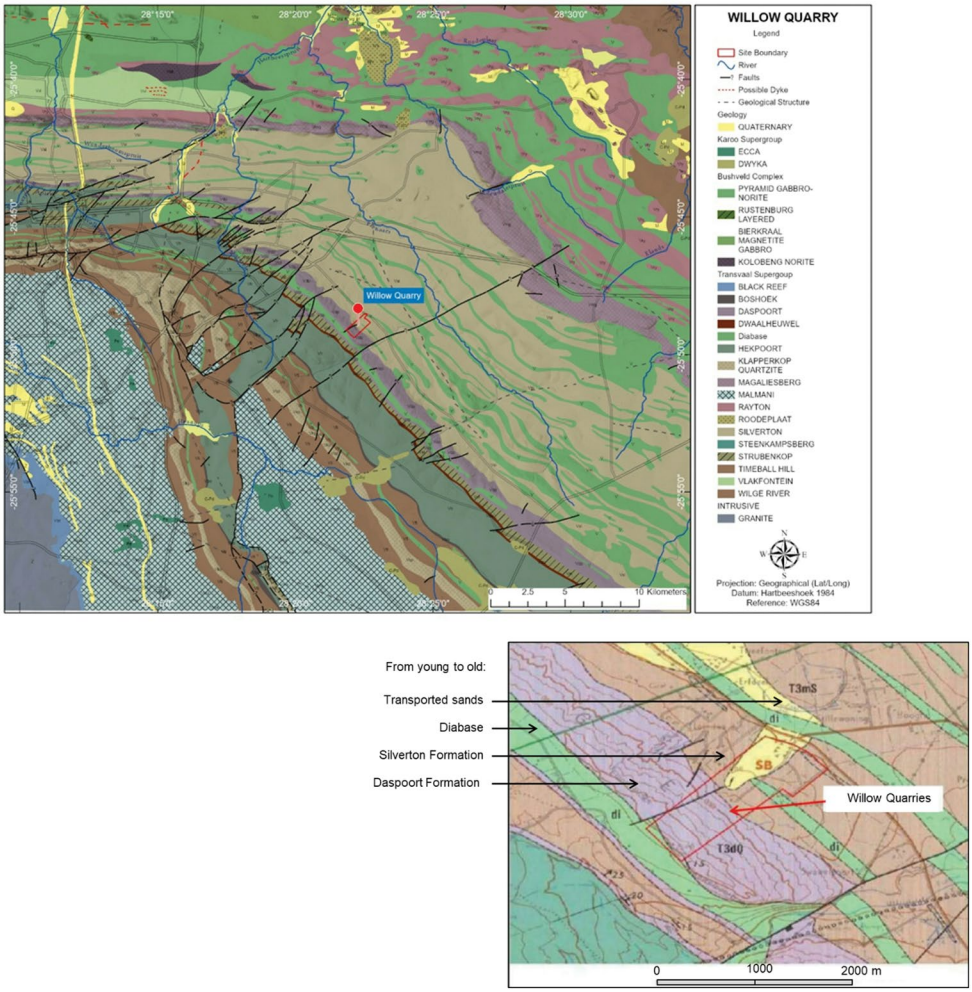

Fig. 2 Regional (top) and site-specific (bottom) geology of the study area

Elevations range from 1 420 m in the northeast to 1 560 m in the southwest (Fig. S2), with a 120 m decrease over a short distance of 800 m sloping north-eastward.

Mining activities have substantially altered the topography, creating steep gradients along the pit edges and stockpiles. Surface runoff enters the excavated areas, contributing to groundwater recharge. The site is largely inward-draining and contributes minimally to external stormwater runoff.

Precipitation and evaporation

The precipitation data were recorded at the Willows rainfall station at the quarry. Long-term records from the South African Weather Service (SAWS) Irene station, located 18 km from the quarry, and from the Department of Water and Sanitation (DWS) were used to extend the time series (Fig. S3). The Pegram et al. (2016) database, which offers raster-based monthly rainfall estimates for Southern Africa, provides a site-specific MAP of 769 mm (Table 2). This comprehensive dataset limits the reliance on data from a single station.

Recharge for the quaternary catchment A23A, based on the GRA II report, is estimated at 8.1% of the total rainfall, corresponding to an annual recharge of 56.6 mm, or approximately 38.6 Mm^3 per year. Evaporation data were sourced from the South African Atlas of Climatology and Agrohydrology (Lynch and Schulze 2006) which provides Class A-pan equivalent evaporation estimates. The site experiences an annual Class A-pan evaporation of 2 156 mm with monthly evaporation rates detailed in Table 2. To adjust for the overestimation caused by pan evaporation being higher than lake evaporation, a correction factor of 0.77 (Linacre 1994) is applied, resulting in more accurate estimates for evaporation from the pit lake.

By using both regional and site-specific data, the precipitation and evaporation values offer a more accurate reflection of the water balance at the quarry.

Geological setting

The study area is primarily underlain by the Daspoort Formation, a prominent member of the Upper Pretoria Group

Fig. 3 (**a**) Seepage face at the contact between the weathered diabase and quartzite near the base of the open pit, as indicated by general wetness of the rock surface; (**b**) water emerging from discrete fractures farther along this same bench; (**c**) the Bronberg Ridge to the south of the quarry pit; and (**d**) the vertical, sub-vertical and horizontal fractures that are typical in the quartzite of the Daspoort Formation

Table 1 Quaternary catchment area characteristics (after Bailey and pitman 2016)

Quaternary catchment	Area	Mean annual precipitation (MAP)	Mean annual runoff (MAR)	Mean annual evaporation (MAE)
A23A	682 km^2	698 mm	42 mm	1 750 mm

within the Transvaal Supergroup, dating back to the late Archaean to early Proterozoic period (2650 to 2025 Ma). This formation predominantly consists of mature quartz arenites, which are hard, cemented sandstones composed mainly of quartz grains, with minor amounts of mudrocks, ironstones, sandstones, pebble arenites, and conglomerates (Eriksson et al. 1993). These quartz arenites are well-exposed along the Bronberg Ridge, a prominent northwest-striking range, reflecting a shallow marine and fluvial depositional environment. The deposition of the Daspoort Formation marks the onset of a major marine transgression, which continued into the subsequent Silverton Formation. Lying unconformably beneath the Daspoort Formation is the Strubenkop Formation, comprising mudstones and siltstones interbedded with fine-grained sandstones. The transition to the Silverton Formation, characterised by carbon-rich shales and tholeiitic lava, is marked by a sharp contact with the Daspoort Formation (Eriksson et al. 2006).

Key geological features include diabase intrusions as sills and dykes, which exploit weak discontinuities within the quartzitic sandstones and have led to significant contact metamorphism, transforming the clastic rocks into quartzites (Eriksson and Reczko 1995). These intrusions, associated with the Bushveld Igneous Complex, created distinct weathering profiles and contributed to northwest-southeast trending folds and faults affecting local geology. The general dip of the rock mass is toward the north, with notable faults intersecting the quarry along its northwestern ramp, impacting both the stability of the quarry walls and potential groundwater flow pathways (Fig. 5).

The Silverton Formation forms a broad plain between the Bronberg Ridge and surrounding ranges, consisting mainly of carbonaceous shales altered into hornfels near contact zones due to diabase intrusions (Eriksson et al. 2006). The

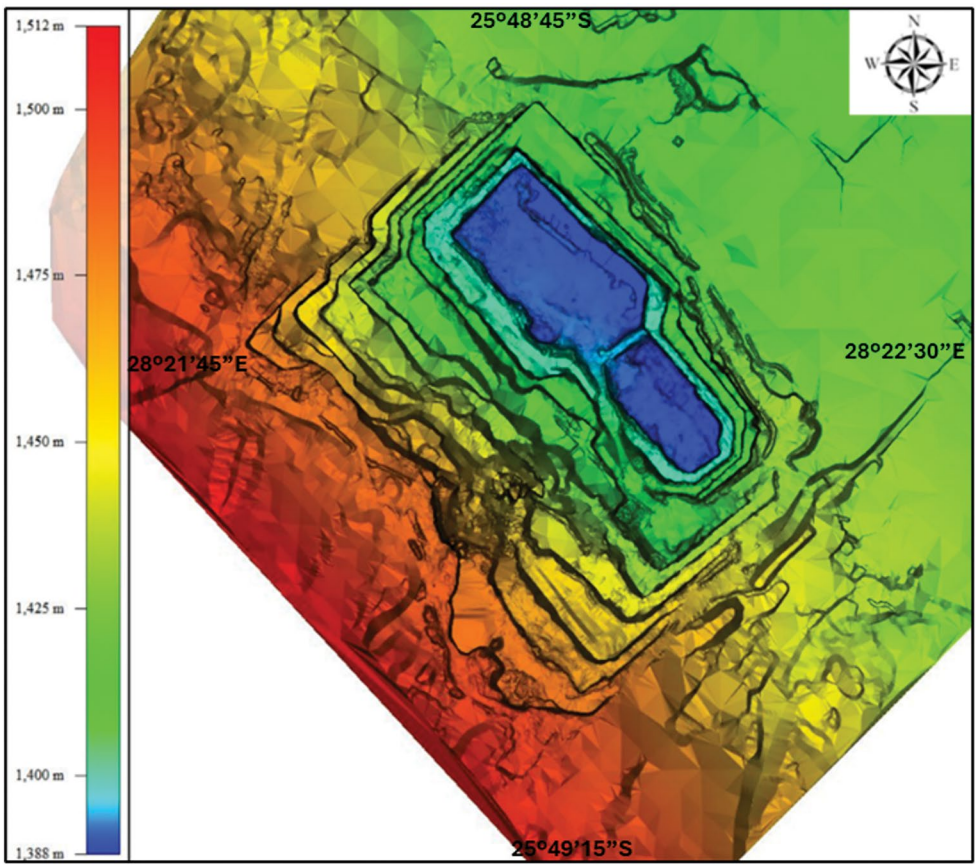

Fig. 4 Digital elevation model depicting the site topography

Table 2 Average monthly rainfall and evaporation rates for the open-pit quarry (Lynch and Schulze 2006)

Month	Rainfall (mm) after Pegram et al. 2016	Class A-pan equivalent potential evaporation (mm)	Lake evaporation after Linacre 1994 (mm)	Rainfall -lake evaporation (ET) (mm)
Jan	149	223	172	-23
Feb	156	183	141	15
Mar	83	183	141	-58
Apr	130	146	112	18
May	5	132	102	-97
Jun	9	108	83	-74
Jul	0	120	92	-92
Aug	0	163	126	-126
Sep	1	203	156	-155
Oct	18	234	180	-162
Nov	151	228	176	-25
Dec	67	233	179	-112
Total	**769**	**2 156**	**1 660**	**-891**

complex geology, characterised by the deposition of quartz arenites and shales, tectonic deformation, and intrusion-related metamorphism, plays a critical role in slope stability and hydrogeological conditions, necessitating careful analysis for quarry operations and groundwater flow.

Fracture characterisation

Present-day stress regime

The stress regime surrounding the study area was determined using six earthquake focal mechanisms from the South African National Seismograph Network (SANSN) (Dhansay 2021). Two faulting regimes normal and strike-slip

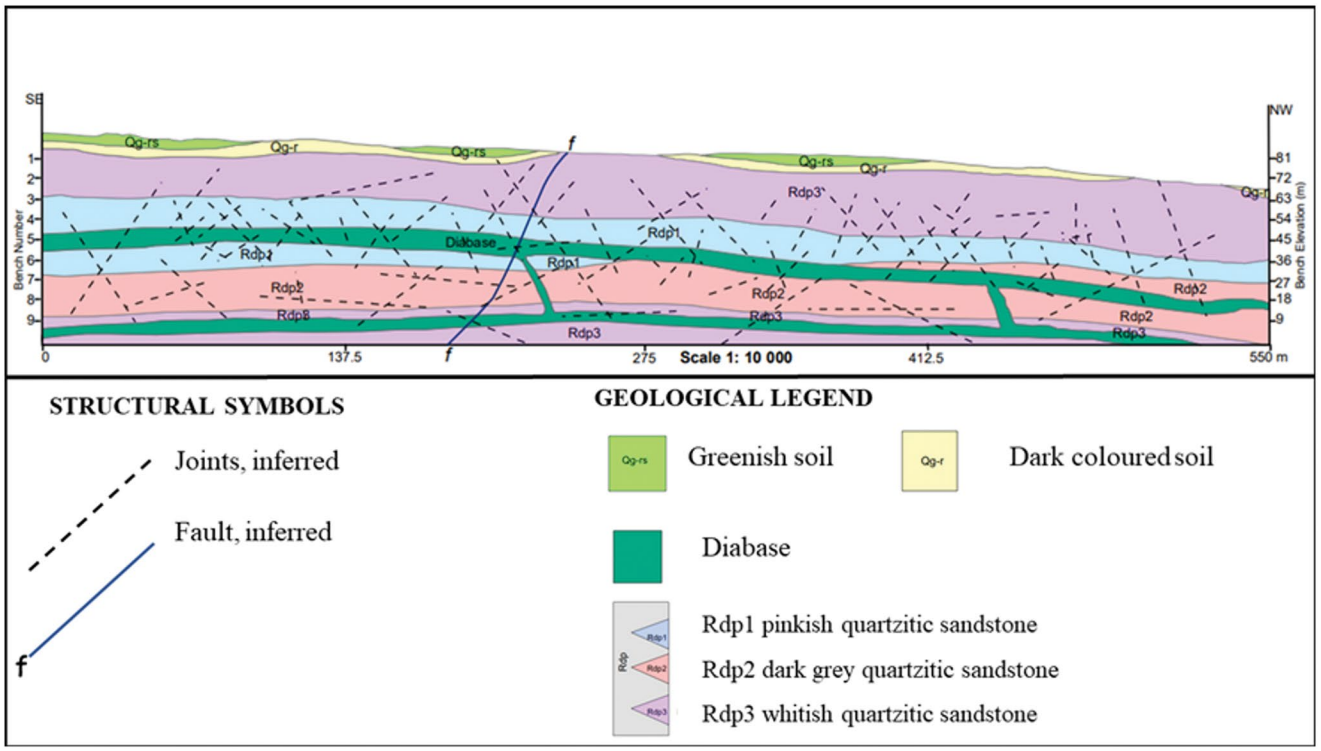

Fig. 5 Geological cross-section of the study area (NW-SE orientation)

Table 3 Present-day stress regime orientation and magnitude for normal and strike-slip faulting near the study area

Regime	Stress	Trend	Plunge	Magnitude (MPa)
Normal	σ1	251.6	2.9	25.02
	σ2	161.2	8.5	19.35
	σ3	1	81	13.68
Strike-slip	σ1	245.6	26.1	34.36
	σ2	113.2	54	25.02
	σ3	347.6	23	15.68

dominate the region, with principal stresses aligned differently in each regime, influencing the local fracture network. Normal faulting is characterised by vertical maximum principal stress (σ1), while strike-slip faulting is dominated by horizontal maximum and minimum principal stresses, σ1 and σ3 (Fig. S4).

Present-day stress magnitude

Present-day stress magnitudes were estimated following (Dhansay et al. 2017) using a bulk rock density of 2 550 kg/m³, pore fluid density of 1 080 kg/m³, and a reservoir depth no greater than 1 000 m. Pore fluid pressure at these depths is estimated at 10.46 MPa. With a coefficient of friction (μ) of 0.85 and a stress ratio R of 0.5, stress magnitudes for normal and strike-slip regimes were calculated. The results are summarised in Table 3.

Fault kinematics

Twenty fault kinematic measurements from the study area reveal predominantly NE-SW and NW-SE oriented fractures, with regional fracture patterns (Dhansay 2021). These faults are generally steeply inclined (75º and 90º), with a few gently inclined faults (Fig. 6).

Reactivation potential

Slip and dilation tendency analyses (Morris et al. 1996) were conducted to evaluate the reactivation potential of faults in both normal and strike-slip faulting conditions (Dhansay et al. 2017). Analysis of fault reactivation potential suggests that moderately inclined NW-SE fractures are most likely to reactivate under normal faulting, whereas steeply inclined NE-SW and NW-SE fractures may reactivate under strike-slip conditions (Fig. S5). This reactivation potential is crucial for understanding fracture dynamics and groundwater movement in the area.

The fracture tracer tests conducted within the blast-damage zone (BDZ) were shaped by the complex interplay of fractures and bedding planes. The BDZ, impacted by quarry blasting, features interconnected fractures that modify tracer movement through the vadose zone. This interaction between fractures and bedding planes offers essential

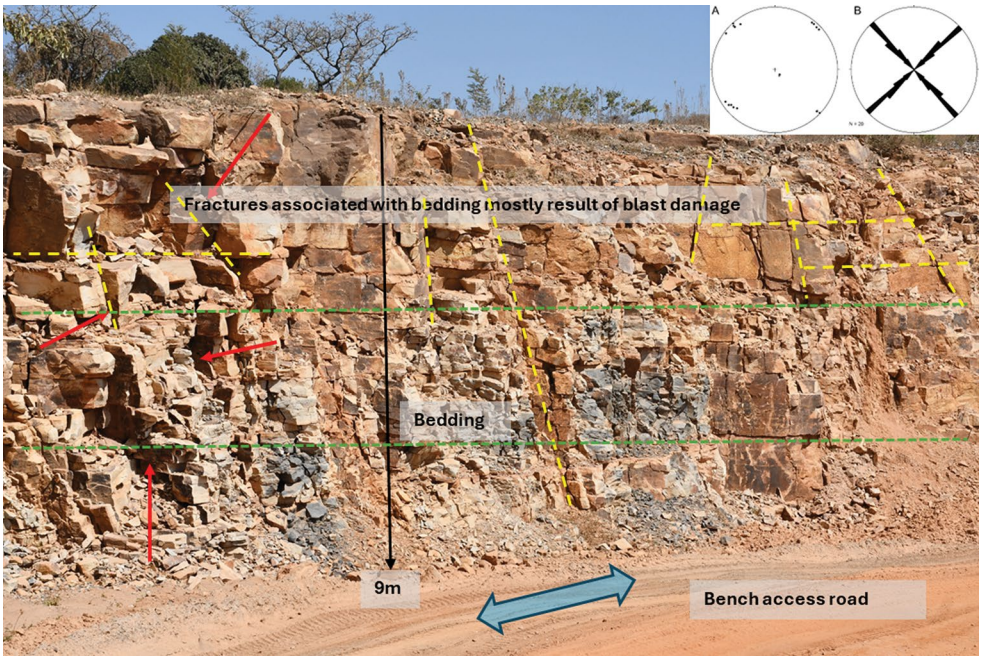

Fig. 6 Fractures associated with bedding, mainly due to blast damage. Inset (**a**) Poles of measured faults; and (**b**) rose diagram showing the predominant fault orientation (photograph by van Wyk, 2023)

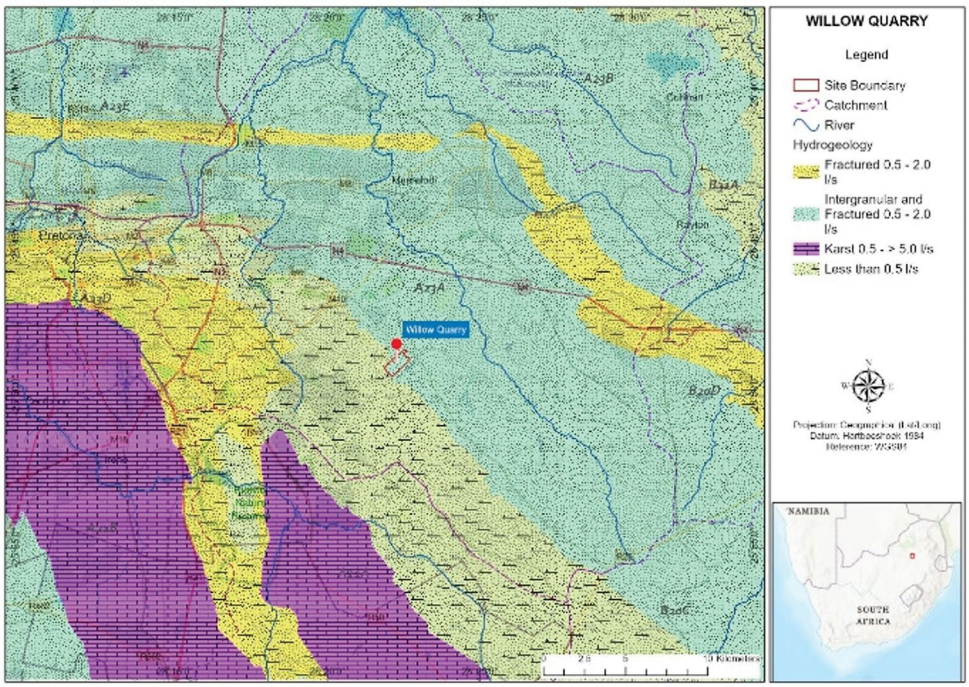

Fig. 7 Map showing regional aquifer yield and classification in the study area, based on the 1:500 000 Hydrogeological Map Series (DWAF 1999)

context for understanding the tracer transport dynamics explored in this study.

Local hydrogeology of the study site

The study area is classified as an intergranular and fractured aquifer system, with borehole yields ranging from 0.5–2.0 L/s (DWAF 1999) as shown in (Fig. 7). Groundwater is stored in fractures within the Daspoort Formation, primarily along NW-SE and NE-SW oriented joints, which significant influence groundwater flow across the Bronberg Ridge. According to (Van der Neut 1990), the Daspoort Formation is less than 100 m thick, while the Pretoria Group, which includes the Daspoort Formation, exceeds 2 000 m in thickness. Barnard (2000) does not classify the Daspoort Formation as an aquifer, indicating that any associated aquifer would be categorised as a 'Minor Aquifer' according to the South African Aquifer System Management Classification (Parsons 1995).

Recharge rates are estimated at 74.3 mm/a, approximately 10.6% of annual rainfall (Vegter 1995). Groundwater levels in borehole WILL-GW-02, fluctuate between 5 m and 25 m below the surface, reflecting seasonal patterns driven by rainfall (Fig. 8).

Groundwater flow in the study area is primarily controlled by structural features, with NW-SE and NE-SW fractures facilitating movement, especially under normal and strike-slip faulting conditions. The Daspoort Formation's limited infiltration and storage capacity can lead to surface water ponding after heavy rainfall.

Materials and methods

Sampling strategy

In total, nine samples were collected at the end of the dry season (April to September 2022) and the beginning of the wet season (October 2022) from both quarry pit water and boreholes (excluding tracer samples). The data indicated limited groundwater usage in the area, with most boreholes serving private landowners for domestic or livestock purposes. Groundwater samples were collected from unequipped boreholes using a 2″ (50 mm) Grundfos MP1 submersible pump (Grundfos South Africa (Pty) Ltd., Johannesburg, South Africa). Each borehole was purged until the physicochemical parameters stabilised. Continuous in situ measurements of temperature, electrical conductivity (normalised to 25 °C), pH, and oxidation-reduction potential were taken using an Aquaread GPS Aquameter (AP-5000) portable multiparameter probe (Aquaread Ltd., Broadstairs, Kent, UK) in a flow-through cell to minimise atmospheric exposure. Alkalinity was determined on-site as $CaCO_3$ (mg/L) with a Hach SL1000 Portable Parallel Analyzer® (PPA) using either low- or high-range total alkalinity Chemkey® reagents (Hach South Africa (Pty) Ltd., Randburg, South Africa). Alkalinity was then converted to HCO_3^- concentrations based on the pH readings. This conversion is reasonable because all samples displayed pH values between 6.5 and 8.2, where bicarbonate is the dominant species contributing to alkalinity (Stumm & Morgan, 1996). Contributions from carbonate (CO_3^{2-}) or carbonic acid (H_2CO_3) were considered negligible in this range.

Analytical methods

Analysis of major and minor ions

Water samples were collected using a 60 mL HENKE-JECT® syringe (Henke-Sass, Wolf GmbH, Tuttlingen, Germany) that was rinsed three times with the sample and filtered with 0.45 µm cellulose acetate (CA) syringe filters into two 60 mL HDPE bottles. The bottle for cation analysis was acidified directly in the field at pH ~ 3 with HNO_3 (Suprapur®, Merck South Africa, Modderfontein, South Africa), Concentrations of major ions (Cl^-, Na^+, K^+, Mg^{2+}, Ca^{2+}, SO_4^{2-}), as well as bromide (Br^-) and phosphate (PO_4^{3-}), were analysed at Waterlab (Pty) Ltd., Pretoria, in accordance with the South African National Standard (SANS) 241-1:2015) using a single-channel ion chromatograph, Metrohm 930 Compact IC Flex (Metrohm SA (Pty) Ltd., Cape Town, South Africa). Anion analysis was performed at 35 °C on a Metrosep A Supp 5–250/4.0 column (Metrohm SA (Pty) Ltd., Cape Town, South Africa) with a flow rate of 0.7 mL/min, using an eluent of 3.2 mM sodium bicarbonate + 1.0 mM sodium carbonate. Cation analysis was carried out at 30 °C on a Metrosep C 6 - A150/4.0 column (Metrohm SA (Pty) Ltd., Cape Town, South Africa) with a flow rate of 0.9 mL/min, using an eluent of 1.7 mM nitric acid + 1.7 mM dipicolinic acid. The repeatability of the analytical method was within 5%, and precision was ensured through the use of certified reference materials and routine calibration of the instrument. Method precision for major ions, expressed as relative standard deviation (RSD), typically ranged between 2 and 5%, depending on the ion concentration, in line with quality control protocols implemented by the accredited laboratory.

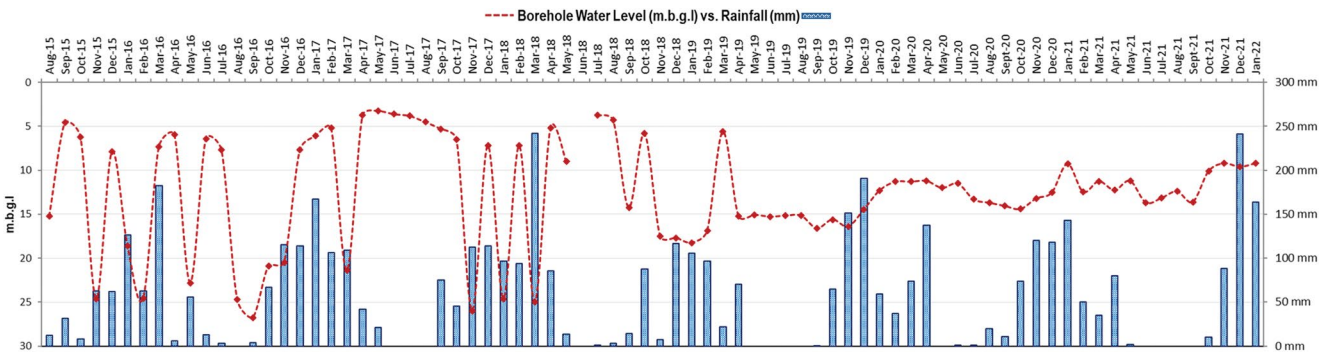

Fig. 8 Groundwater levels in monitoring borehole WILL-GW-02 and corresponding rainfall data from 2015–2021

Sample analysis for stable and radioactive isotopes

Samples were analysed for δ^2H, $\delta^{18}O$, d-excess, and tritium (^3H) content. All $\delta^{18}O$ and δ^2H values are reported relative to the Vienna Standard Mean Ocean Water (VSMOW), as referred to by Mook (2000). In total, nine water samples were submitted to iThemba LABS (Johannesburg, South Africa) on 30 November 2022 for analysis. The samples were analysed using a Los Gatos Research Liquid Water Isotope Analyzer (Los Gatos Research (LGR), a member of the ABB Group, San Jose, California, USA), with precision estimated at 0.5‰ for $\delta^{18}O$ and 1.5‰ for δ^2H. Results are expressed in δ-notation relative to VSMOW. The samples for tritium were distilled and subsequently enriched by electrolysis using a special set-up consisting of two concentric metal tubes, one made of stainless steel serving as the outer anode and container, and the other made of mild steel with a special surface coating serving as the inner cathode. After introducing 500 mL of the water sample containing sodium hydroxide into the cell, a direct current of 10–20 A was passed through the cell, which was then cooled due to heat generation. Following several days, the electrolyte volume was reduced to 20 mL, resulting in a 25-fold volume reduction and a corresponding tritium enrichment factor of approximately 20. To verify the enrichment attained, samples of standard known tritium concentration (spikes) were run in one cell of each batch. For liquid scintillation counting (LSC), samples were prepared by directly distilling the highly concentrated electrolyte. A mixture of 10 mL of the distilled water sample and 11 mL of Ultima Gold (scintillation cocktail) was placed in a vial and counted using a PerkinElmer Tri-Carb 3170TR/SL Liquid Scintillation Analyzer (PerkinElmer (Pty) Ltd., Midrand, South Africa) for two to three cycles of 4 h each. The detection limit for enriched samples was 0.3 TU (tritium unit).

Results

Hydrochemical characteristics

Groundwater samples from locations, WILL-GW-01, WILL-GW-02, and FARM-B1 exhibit a calcium-magnesium-bicarbonate facies, indicative of minimal chemical alteration. In contrast, WILL-PIT-01 and WILL-PIT-02 quarry pit water samples show elevated concentrations of sulphate. The increased sulphate levels likely result from the geochemical interactions within the quarry environment, possibly influenced by mining activities or local geology. The groundwater and quarry pit water sampling points are indicated on the map in Fig. 9, and the Piper diagram representing the hydrochemical facies of the groundwater and quarry pit water samples is shown in Fig. 10, which highlights the distinct water types present in the study area. The difference in water chemistry between the groundwater and quarry pit water samples emphasises the importance of site-specific water quality assessments, especially in areas impacted by anthropogenic activities such as quarrying.

Two distinct hydrochemical facies were identified: a calcium-magnesium-bicarbonate type in most groundwater samples, indicating relatively fresh and shallow groundwater, and a calcium-magnesium-sulphate type in the quarry

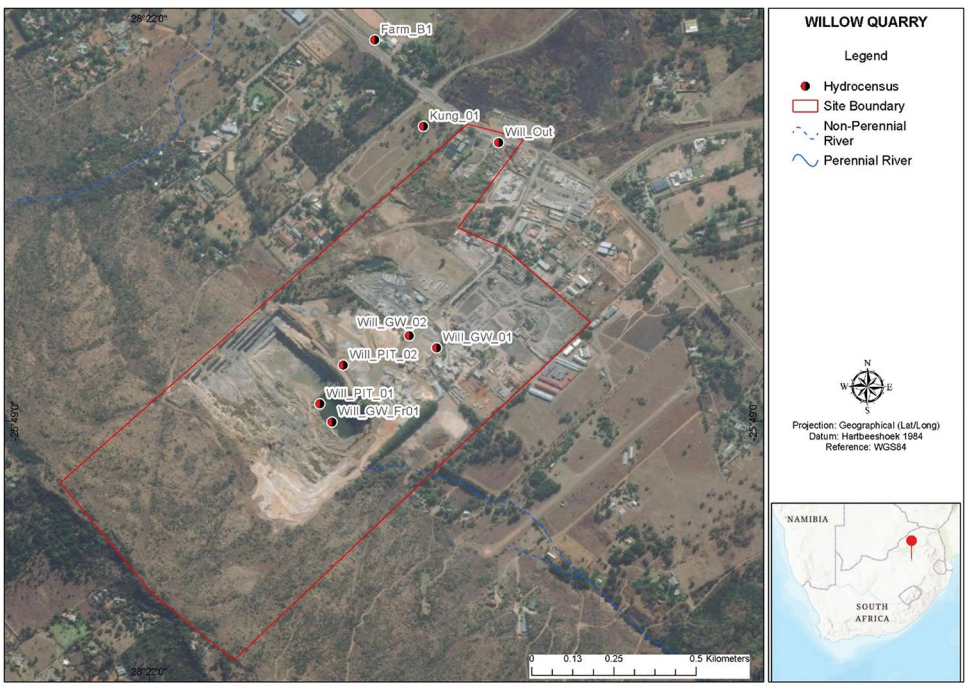

Fig. 9 Map of the study area showing the locations of groundwater and quarry pit water sampling points

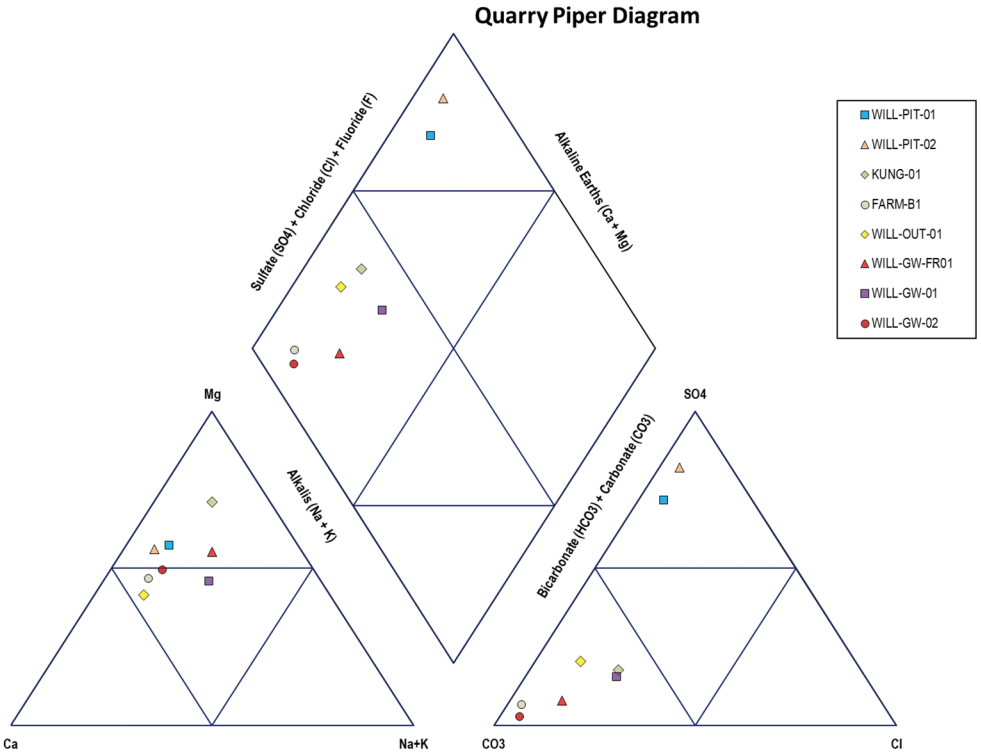

Fig. 10 Piper diagram representing the hydrochemical facies of quarry pit water and groundwater samples

Table 4 Isotopic composition and hydrological parameters of water samples from the quarry site

Sample ID	Date	Latitude (DD)	Longitude (DD)	δ ^{2}H‰	δ^{18}O‰	D-Excess‰	TU	±	Elevation (m a.s.l.)
WILL-GW-01	2022/10/28	-25.8146667	28.374527	-21.8	-4.21	11.88	0.5	0.2	1425
WILL-GW-02	2022/11/04	-25.8143333	28.373777	-21.6	-4.36	13.28	0.4	0.2	1430
WILL-GW-FR01	2022/10/29	-25.8166944	28.371666	-22.1	-4.63	14.94	1	0.2	1398
FARM-B1	2022/10/28	-25.80625	28.372833	-23.0	-4.70	14.67	0	0.2	1408
WILL-PIT-01	2022/10/29	-25.8161944	28.371333	-5.8	-1.23	4.04	1.1	0.3	1397
WILL-PIT-02	2022/10/28	-25.8151389	28.371972	-8.7	-2.12	8.26	1	0.3	1423
KUNG-01	2022/11/04	-25.8086111	28.374166	-18.2	-3.88	12.84	1	0.3	1412
WILL-OUT	2022/10/28	-25.8090556	28.376222	-19.6	-4.09	13.12	1	0.2	1407
RAINWATER	2022/12/07	-25.8150748	28.3738945	-32.0	-5.43	11.44	2.3	0.3	1424
Min				-32.0	-5.4	4.0	0.0		
Max				-5.8	-1.2	14.9	2.3		
Mean				-19.2	-3.85	11.61	0.9		

pit water, likely resulting from the dissolution of sulphide minerals, including pyrite (Fig. 10). Additionally, the presence of an old, now inactive general domestic waste disposal site in the vicinity may be making a significant contribution to the contamination plume, potentially overshadowing the effects of pyrite dissolution. Leachate from domestic waste disposal sites is known to introduce a wide range of contaminants, including nitrate, chloride, sulphate, heavy metals, and organic compounds, which can significantly alter groundwater quality and hydrochemistry (Christensen et al. 2001; Mor et al., 2006; Khan et al., 2022). The influence of such leachate plumes has been widely documented to result in more complex and persistent contamination signatures than those caused solely by natural geochemical processes like pyrite oxidation.

Stable isotope analysis

The $\delta^{18}O$ and $\delta^{2}H$ values ranged from −5.40‰ to -1.20‰ and −32.0‰ to -5.80‰, with mean values of -3.85‰ and −19.20‰ respectively, providing a representative isotopic signature for the study area (Table 4).

The Global Meteoric Water Line (GMWL) (Craig 1961) was used as a reference, but the Pretoria Meteoric Water Line (PMWL) was derived from the Global Network of Isotopes in Precipitation (GNIP) dataset for local interpretation ($\delta^{2}H = 6.7\delta^{18}O + 7.2‰$). Additionally, a Local Evaporation Line (LEL) for quarry pit water samples was established ($\delta^{2}H = 3.26\delta^{18}O - 1.79‰$). Samples WILL-GW-01, WILL-GW-02, WILL-GW-FR01, FARM-B1, KUNG-01, and

WILL-OUT clustered along the PMWL and GMWL, indicating direct recharge from local rainfall with high d-excess values (mean = 11.6‰), as illustrated in Fig. 11. In contrast, quarry pit water samples (WILL-PIT-01 and WILL-PIT-02) were enriched in δ^2H and $\delta^{18}O$ and showed lower d-excess values, indicating evaporation prior to recharge. The steep slope of the LEL (3.26), calculated from quarry pit water samples that have undergone evaporation, reflects significant evaporation effects under low humidity conditions.

Deuterium excess

Deuterium excess (d-excess) is a second-order isotopic parameter that reflects the difference between the isotopic composition of precipitation and water vapour (Dansgaard 1964). It is calculated as shown in Eq. 1.

$$d = \delta^{2}H - 8 \bullet \delta^{18}O \quad (1)$$

High d-excess values, typically above 10‰, indicate moisture originating from regions with high evaporation rates such as arid zones or zones under conditions of atmospheric recycling (Clark and Fritz 1997; Bowen and Revenaugh 2003).

The relationship between $\delta^{18}O$ and d-excess is illustrated in Fig. 12, highlighting the difference in isotopic composition between groundwater and quarry pit water.

D-excess values:

- Range from 4.04‰ to 14.94‰, with a mean of 11.61‰, suggesting a relatively high evaporation rate from the moisture source (Table 4).

Cluster I groundwater samples (e.g., WILL-GW-01, WILL-GW-02, WILL-GW-FR01, FARM-B1, KUNG-01):

- Exhibit high d-excess values.
- Indicate recharge from rainfall that underwent significant evaporation under low humidity and temperature conditions.

Cluster II quarry pit water samples (e.g., WILL-PIT-01 and WILL-PIT-02):

- Display lower d-excess values.
- Reflect potential evaporation or water-rock interaction processes, likely contributing to the heavy isotope enrichment observed in these samples (Kendall and McDonnell 2012).

Groundwater samples show higher d-excess values compared to quarry pit water samples, consistent with the low infiltration capacity of the Daspoort Formation.

Tritium analysis

The tritium values of water samples in the study area were found to range from 0.0 to 2.3 TU, with a mean of 0.9 TU (Table 4). Groundwater samples exhibited tritium concentrations of between 0.4 and 1 TU, suggesting relatively

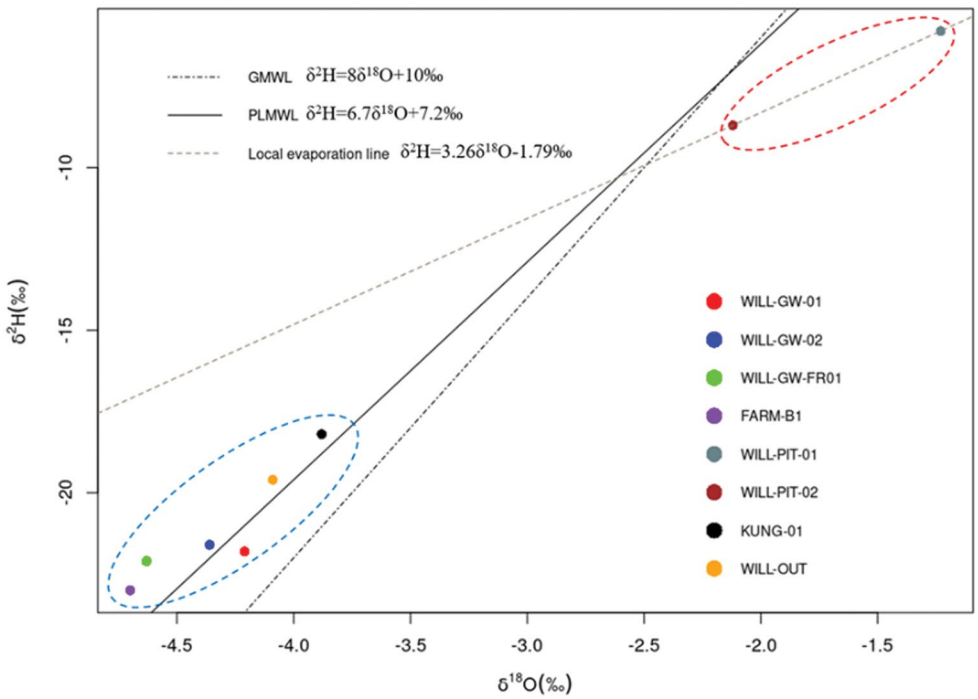

Fig. 11 δ^2H vs. $\delta^{18}O$ plot showing isotopic variation of quarry pit water and groundwater samples relative to the Pretoria Local Meteoric Water Line (PLMWL) and the Global Meteoric Water Line (GMWL)

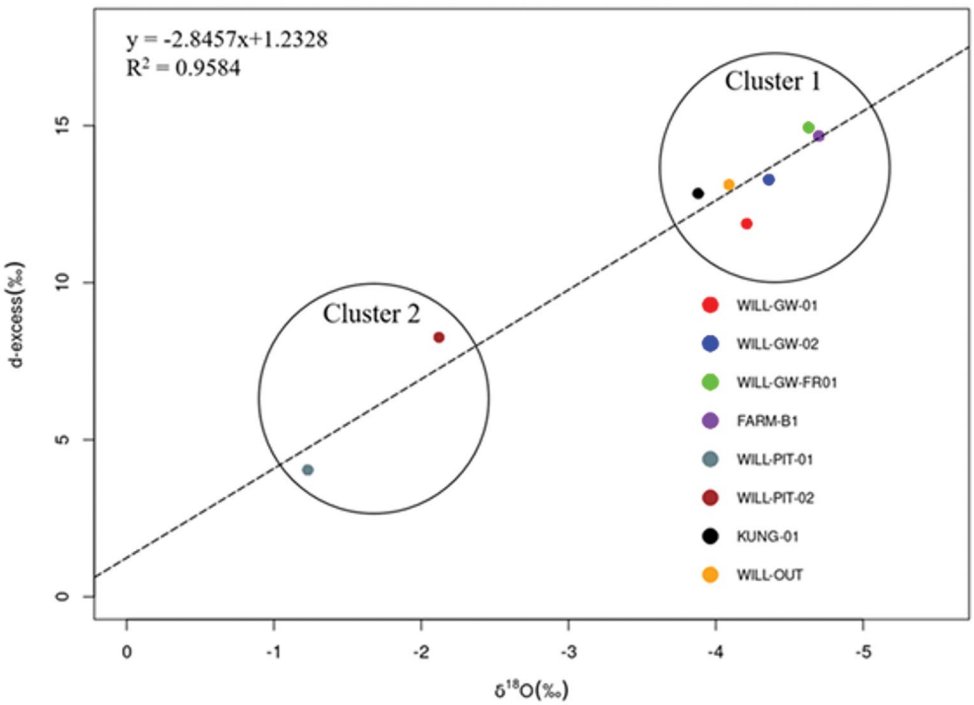

Fig. 12 Cross-plot of d-excess vs. $\delta^{18}O$ for water samples from the study area

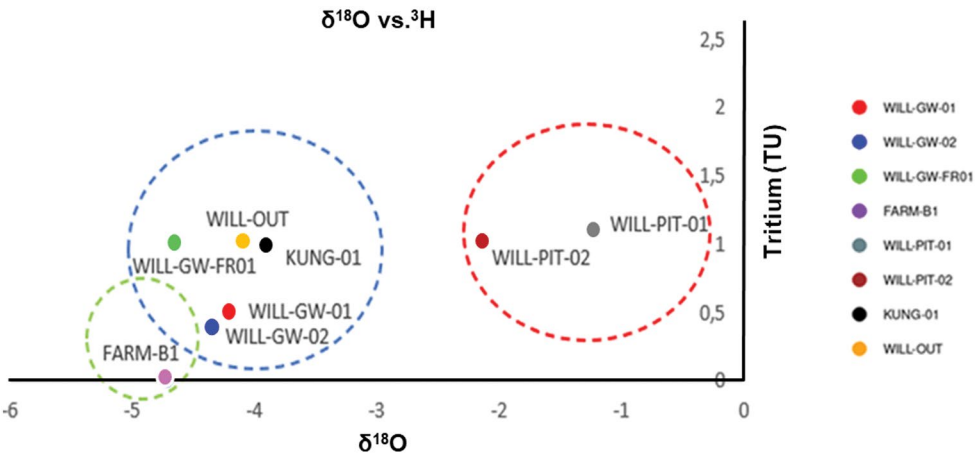

Fig. 13 Relationship between $\delta^{18}O$ (‰) and tritium (^3H, TU) for water samples in the study area

older water or a mix of old and recent (young) recharge. Quarry pit water samples (WILL-PIT-01, WILL-PIT-02) were found to have tritium values of 1 to 1.1 TU, indicating more recent recharge (Fig. 13).

Overall, the isotopic signatures and d-excess values suggest direct recharge from local rainfall, further supported by tritium data, which point to young, recently recharged waters.

Artificial tracers

In February and August 2023, two artificial tracer experiments using fluorescent dyes were carried out on the quarry site. Both experiments used the same injection point (borehole BH.3) and the same monitoring point (M-1), approximately 6 m apart. The M-1 monitoring point was selected as the only natural flow/discharge point (0.9 L/s) in the quarry, located at the contact between quartzite and weathered diabase on the lowest bench of the pit (Fig. 14). This point was equipped with a GGUN-FL30 fluorometer, providing real-time detection and recording of breakthrough data (Fig. 15). The purpose of repeating this experiment was to investigate the changes potentially induced by two external factors: (1) hydrological conditions (rainy or dry season); and (2) blasting operations that took place in the quarry between the two tracer tests.

The first (rainy season) tracer test was carried out on 8 February 2023. The water level in borehole BH.3 was 4 m b.g.l. (metres below ground level). Rhodamine WT (4.7 g) was injected into the borehole, followed by 0.5 L of flush

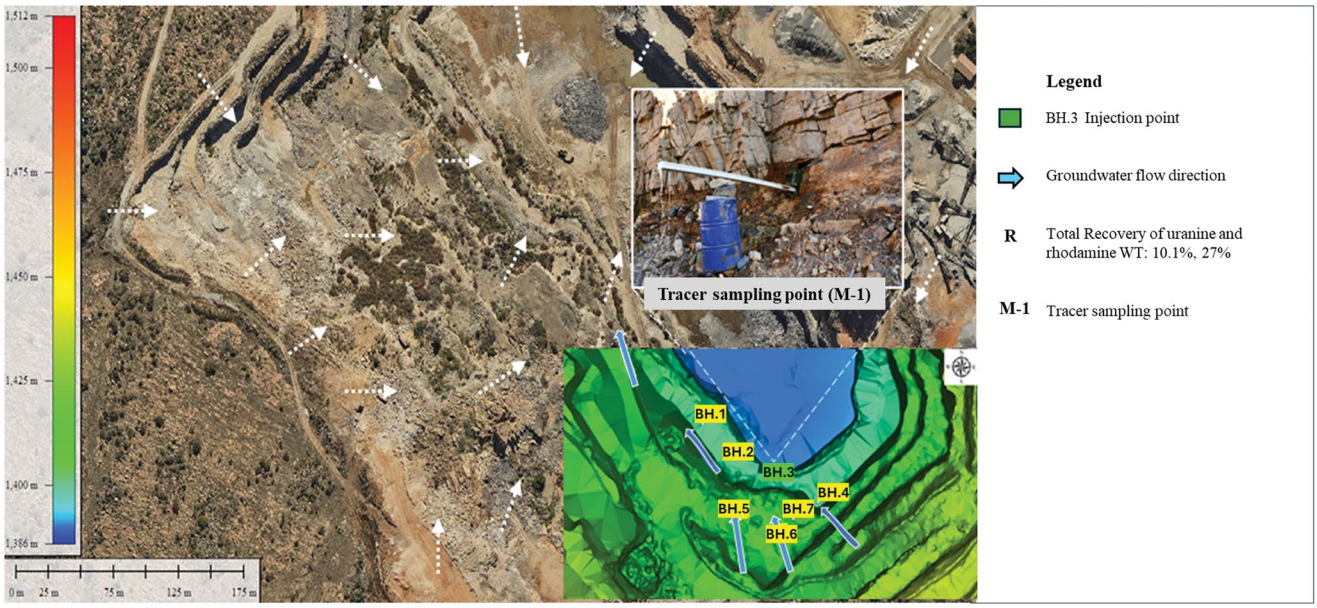

Fig. 14 Injection points and sampling location used during the tracer tests

Fig. 15 Experimental set-up for tracer monitoring using the GGUN-FL30 fluorometer (photographs by van Wyk, 2023)

fluid. Tracer breakthrough at monitoring point M-1 occurred at 2 488 s, with a dominant flow velocity of 10.8 m/h and a recovery rate of 27%. The breakthrough curve (BTC) displayed multiple peaks, indicating the presence of several flow paths within the fracture network (Fig. 16). Characteristic BTC times and velocities are summarised in Table 5.

The second (dry season) tracer test was performed on August 9, 2023. The depth of the water level in BH.3 was 5.1 m b.g.l. Uranine (2 g) was injected into the borehole followed by 1 L of flush fluid. Initially, no tracer breakthrough was observed. Three additional 85 L flushes were successively applied to mobilise the injected tracer, this time leading to a positive breakthrough logically marked by three concentration peaks (Fig. 17). It should be noted, however, that despite the three flushes, the overall recovery rate was only 10.1%, significantly lower than in the first experiment. This lower recovery rate is likely due to a larger spatial divergence of flows from the injection point, related to the much higher total flush volume. Characteristic BTC times (corrected for successive flushing times) and velocities are summarised in Table 5 for easy comparison with the first experiment.

The data obtained from these tracer tests, as illustrated in Table 5, will be further interpreted and analysed, focusing on analytical modelling.

Bodin (2020) developed MFIT (Multi-Flow Inversion of Tracer breakthrough curves) version 1.0.0, which is an open-source tool designed for interpreting complex breakthrough curves (BTCs), including multi-peak and heavy-tailed distributions. The MFIT software models solute transport through discrete one-dimensional channels representing primary flow paths in fractured systems (Fig. 18). It applies four analytical models—MDMi, MDMed, SFDM, and 2RNE—each based on distinct analytical solutions to the advection-dispersion equation (ADE). Immobile porosity can cause the advection-dispersion equation (ADE) equation to fail at predicting solute transport; dual-domain mass transfer (DDMT) models were developed as a modification of the ADE to represent immobile pathways; immobile porosity is one of the parameters of DDMT models that describes domains of low advective velocity. The MDMi and MDMed models assume that tracer transport occurs via single-porosity, one-dimensional flow paths, while the SFDM and MDP-2RNE models incorporate dual-porosity flow paths, simulating mass exchange between mobile and immobile zones. Specifically, the MDP-2RNE model is based on a first-order mass exchange process, whereas the SFDM model assumes a second-order diffusion-based process (parallel-plate channel geometry). The MFIT software also integrates PEST for regularised inversion and uncertainty analysis of model parameters, as detailed by Bodin (2020) and (White et al. 2014). The total discharge rate ($Q = 3.24$ m³/h) was fixed before inversion, with parameters such as tracer mass (M), mean transit time (t_0), Péclet number (Pe), proportion of mobile porosity (Ψ_1), and first-order mass transfer coefficient (ω_1) optimised to accurately model tracer transport dynamics.

As shown in Fig. 19, corresponding to Test 1 in Table 5, the inverted breakthrough curves (BTCs) for models with four (4) and 12 flow channels align closely with the experimental data. This fit informs the parameter values listed in Table 6. Figure 19 also depicts the PHI vs. N curves, illustrating the results of the PEST optimisation method with varying channel numbers. Both MDMi and MDP-2RNE models demonstrate proficiency in representing the underlying flow mechanisms. The optimal channel numbers were determined by evaluating the trade-off between model complexity and fit to the observed data. For the MDMi model,

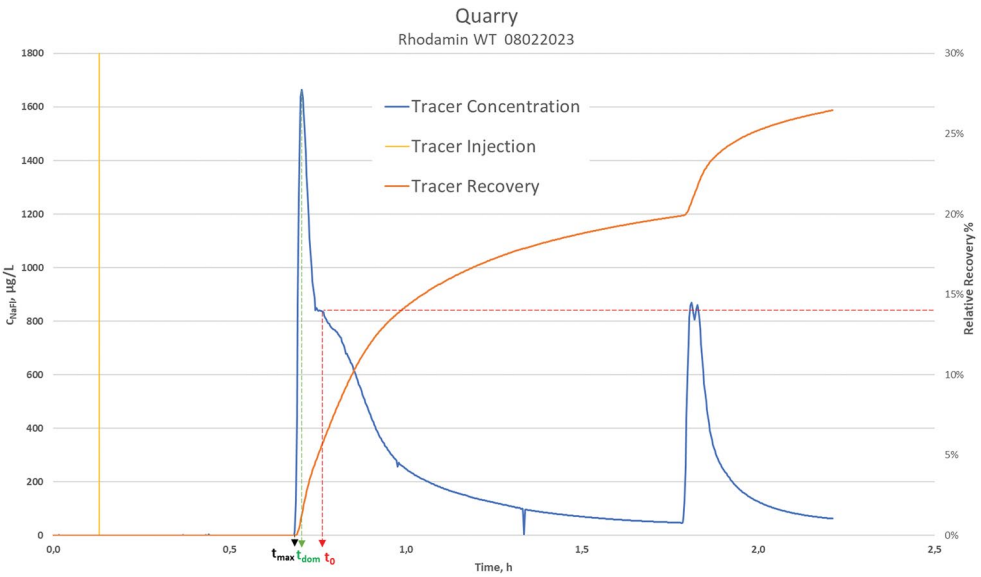

Fig. 16 Breakthrough and recovery curves for rhodamine WT during the wet season

Table 5 Summary of tracer tests and results at the quarry site. Maximum flow velocities (v_{max}) were calculated based on the time of first tracer detection (t_0). Dominant transit times (t_{dom}) and velocities (v_{dom}) were determined using the main breakthrough point and peak concentration (c_p). Note that the breakthrough curves for different tests are presented separately, as they were not superimposed

Test code	Date	Tracer used	Mass injected (g)	Flushing	Flushing volume (L)	Observation point(s)	Nature of flow	Flow rate (L/s)	Season	Distance to M-1 (m)	t_{max} (s)	t_{mean} (s)	t_{dom} (s)	v_{max} (m/s)	v_{mean} (m/s)	v_{dom} (m/s)	Recovered mass (%)
Test 1	February 8, 2023	Rhodamine WT	4.7	Yes	0.5	M-1	Natural	0.9	Wet	6.05	2488	2700	2520	0.002	0.002	0.002	27
Test 2a*	August 9, 2023	Uranine	2	Yes	85	M-1	Natural	0.9	Dry	6.05	238	706	526	0.025	0.009	0.012	10.1
Test 2b*	August 9, 2023	Uranine	0	Yes	85	M-1	Natural	0.9	Dry	6.05	1917	2277	2097	0.003	0.003	0.003	7.6
Test 2c*	August 9, 2023	Uranine	0	Yes	85	M-1	Natural	0.9	Dry	6.05	293	643	391	0.021	0.009	0.016	1.8

*Indicates a series of tests stemming from a single tracer injection of uranine, followed by staggered flushes to observe tracer recovery at M-1

the identification of 12 paths is based on comprehensive analysis, although this choice may not be immediately obvious from the PHI(N) curve. In the case of the MDP-2RNE model, the 4-path configuration was found to provide an adequate fit to the data while maintaining simplicity. The inflection point observed on the PHI(N) curve supports this choice, indicating that the 4-path model effectively captures the essential flow dynamics without introducing unnecessary complexity. This suggests that the injected mass splits into independent paths that converge at the output, complicating the fitting of single-flow-path models.

Although the BTCs from both the MDMi and MDP-2RNE models appear almost identical, the underlying conceptual differences between these models are crucial to gain an understanding of the transport mechanisms. The MDMi model explains tracer transport by incorporating multiple low-velocity paths to account for heterogeneous flow conditions. In contrast, the MDP-2RNE model explicitly distinguishes between mobile and stagnant zones, which are not directly represented in the MDMi model. When fewer flow paths are required in MDP-2RNE compared to MDMi for the same tracer test, it suggests that the tracer has interacted with stagnant or very low-flow zones. In the MDMi model, this behaviour is accounted for by adding more slow-moving paths to fit the experimental curve. While both models provide similar information regarding the coexistence of fast and slow paths, the MDP-2RNE model more accurately reflects the influence of stagnant zones in fractured media.

In the analysis of the tracer tests using Model 1 (MDMi), two sets of parameters—mean transit times (t_0) and Péclet numbers (Pe)—were considered to capture the transport behaviour in the fractured quarry. For Model 1 (MDMi), mean transit times (t_0) range from approximately 0.698 to 2.043 h, with Pe values indicating a transition from advection-dominated to dispersion-dominated behaviour. For Model 2 (MDP-2RNE), mean transit times (t_0) vary from 0.689 to 1.821 h, displaying a broader range of Pe values. Both models exhibit similar velocities, averaging 2.0×10^{-3} m/s, while the longitudinal dispersivity (α) indicates a low degree of dispersion ranging from 1.8×10^{-6} m to 1.7×10^{-1} m. It is important to note that α here refers to longitudinal dispersivity, not to the first-order mass transfer coefficient α_j [T^{-1}] as discussed in (Bodin 2020). Although the SFDM model is not displayed in Fig. 19, it was found to perform comparably in model fit to the MDP-2RNE model, which utilises a dual-porosity approach incorporating stagnant water regions and flowing channels, thereby enhancing model behaviour by accounting for peak concentrations while minimising dispersivity effects.

Distinguishing between first and second-order diffusion without independent experiments is challenging. However, irrespective of the shape of the curves, the linear flow

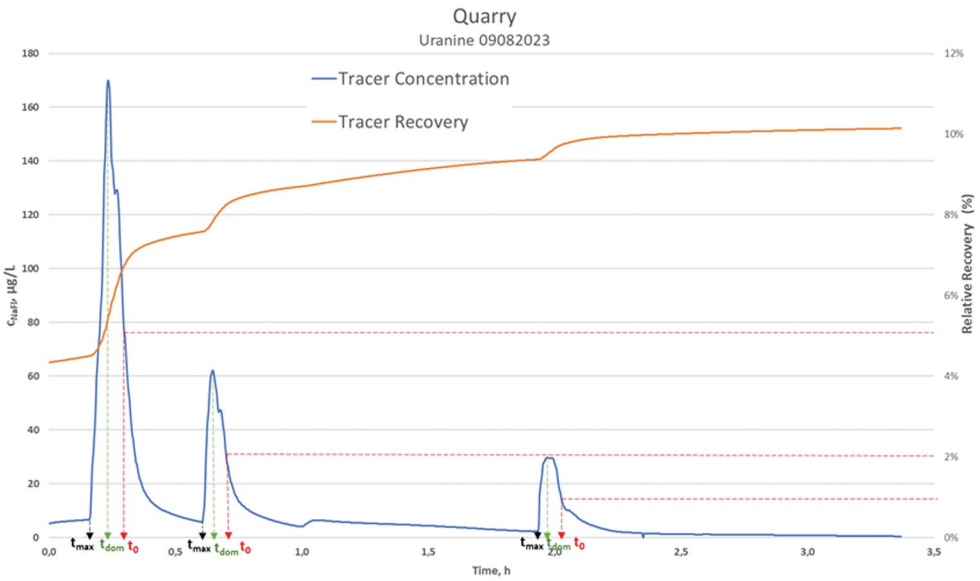

Fig. 17 Breakthrough and recovery curves for uranine during the dry season

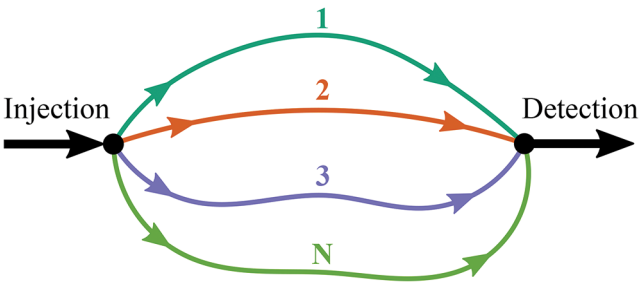

Fig. 18 Conceptual model of the (generic) multi-flow modelling approach in MFIT (Bodin 2020)

velocity was calculated by dividing the length of the flow channel (L) by the maximum travel time (T_{max}) of the tracer as shown in Eq. 2.

$$L/T_{\max} = 6.5\text{m}/2.2\text{h} = 3\ \text{m/h} \quad (2)$$

This indicates a flow velocity considerably higher than the typical velocities associated with molecular diffusion processes, which are generally below millimetres per hour. This suggests that the hypothesis of substantial influence from diffusion on the tracer test can be ruled out, reinforcing the notion that the observed breakthrough patterns are primarily driven by advective transport rather than diffusion mechanisms. Therefore, the focus remains on the dual-porosity model (MDP-2RNE), highlighting the significance of stagnant and mobile water exchange within fractures.

For the BTC obtained in the dry season, the model fit focused on the first peak only, as peaks 2 and 3 are only due to the succession of flushes and therefore contain no additional information. Furthermore, peaks 2 and 3 may have been influenced by previous flushing, which could bias their analysis. The inverted BTC in Fig. 20 demonstrates a strong fit to the experimental data, particularly with four flow channels (N=4). The parameters used for the second tracer simulation are summarised in Table 7. The total discharge rate Q was fixed at 3.24 m³/h to facilitate post-comparison of inverted mass values. Parameters such as tracer mass (M), mean transit time (t_0), Péclet number (Pe), mobile water fraction (Ψ_1), and first-order mass transfer coefficient (ω_1) were optimised.

The last channel is primarily responsible for the tailing observed in the BTC, highlighting the role of delayed tracer transport through specific fracture pathways. These results serve as the basis for the subsequent analysis of transport dynamics within the dry season conditions. The mean transit times ranged from 0.112 to 0.184 h (average: 0.15 h), providing an indication of how rapidly the tracer moved through the primary flow paths of the system. This reflects the advective transport conditions of the system, where the tracer experiences minimal interaction with the matrix during its transit through fractures. Simultaneously, the Pe numbers, which ranged from 8.7 to 287.6, suggest varying degrees of advection-dominated transport. Higher Pe numbers indicate a stronger dominance of advection over dispersion.

For Model 2 (MDP-2RNE), the mean transit times ranged from 0.106 to 0.168 h, with an average of 0.13 h, indicating a similar pattern to Model 1, where advective transport continued to dominate flow within the system. The Pe numbers for this model ranged between 14.6 and 363.0, closely aligning with the values of Model 1, which further reinforced the significance of advection in transporting the tracer. Similar to the observations in Model 1, both velocity and dispersivity values showed consistent flow and dispersion behaviour, which indicated minimal variability between the two models. This finding also reflected minimal exchange between

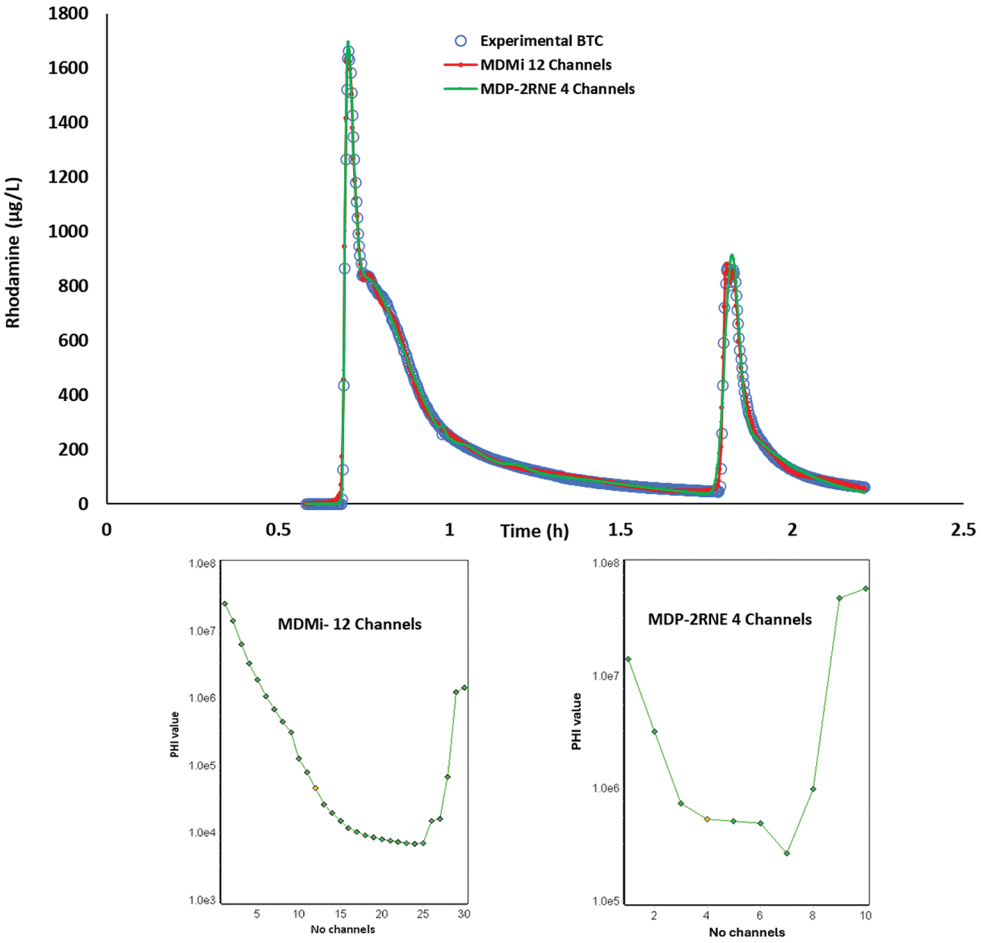

Fig. 19 Wet season BTC fitting analysis using MDMi and MDP-2RNE models for Test 1 with varying channel numbers (*N*). PHI represents the fitting error (sum of squared errors between BTC and model-simulated curve) minimised using PEST inversion routines

Table 6 Optimised model parameters that correspond to the inverted BTC

Model 1 MDMi (ADE instantaneous injection)								
T_{min}	T_{max}	No. Time Steps	Q (m^3/h)	Distance (m)				
0.58	2.21	500	3.24	6.5				
	Channel *(N)*	Mass (g)	t_0 (h)	*Pe*	V (m/s)	α (m)	ψ_1	ω_1 (m^{-1})
	1	31732.3	0.698	42701.5	2.6E-03	1.5E-04		
	2	58484.4	0.708	17807.0	2.6E-03	3.7E-04		
	3	70567.8	0.722	6938.3	2.5E-03	9.4E-04		
	4	102820.1	0.754	1591.2	2.4E-03	4.1E-03		
	5	238388.7	0.821	447.8	2.2E-03	1.5E-02		
MDMi	6	184462.7	0.944	151.1	1.9E-03	4.3E-02		
	7	260151.0	1.295	39.1	1.4E-03	1.7E-01		
	8	31209.6	1.805	125457.3	1.0E-03	5.2E-05		
	9	67885.3	1.825	35945.2	9.9E-04	1.8E-04		
	10	47194.5	1.851	13464.3	9.8E-04	4.8E-04		
	11	49088.9	1.905	3293.8	9.5E-04	2.0E-03		
	12	126470.1	2.043	288.9	8.8E-04	2.3E-02		
Model 2								
	1	89620.2	0.689	3,581,865	2.6E-03	1.8E-06	0.98	0.91
	2	187671.0	0.978	39768.57	1.8E-03	1.6E-04	0.67	0.77
	3	646041.8	0.716	6695.117	2.5E-03	9.7E-04	0.84	0.39
MDP-2RNE	4	21424.5	1.047	3759.173	1.7E-03	1.7E-03	0.92	0.30

T_{min} and T_{max} are the minimum and maximum time values, respectively, for the BTC obtained

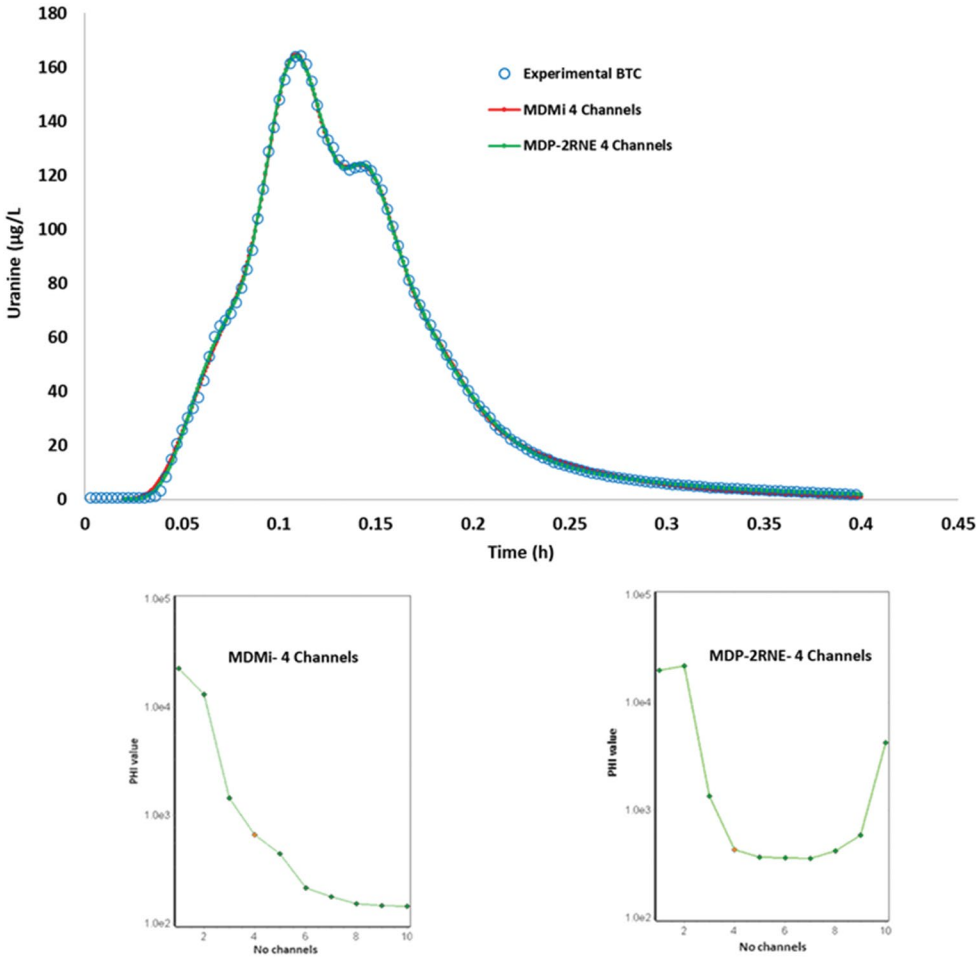

Fig. 20 Dry season inversion solutions of BTC fitting analysis for tracer Test 2a using MDMi and MDP-2RNE models for varying channel numbers (*N*)

Table 7 Optimised model parameters that correspond to the inverted BTC

Model.1 MDMi (ADE instantaneous injection)								
T_{min}	T_{max}	No. time steps	Q (m^3/h)	Distance (m)				
0.02	0.4	500	3.24	6.5				
	Channel (*N*)	Mass (g)	T_0 (h)	*Pe*	*V* (m/s)	α (m)	ψ_1	ω_1 (m^{-1})
	1	9427.8	0.112	120.7	1.6E-02	5.4E-02		
	2	1956.8	0.184	287.6	9.8E-04	2.3E-02		
MDMi	3	6283.8	0.150	228.4	1.2E-02	2.8E-02		
	4	35431.9	0.140	8.7	1.3E-02	7.5E-01		
Model.2								
	1	23458.2	0.105	14.6	1.7E-02	4.5E-01	0.86	0.05
MDP-2RNE	2	13315.7	0.111	115.6	1.6E-02	5.6E-02	0.96	0.07
	3	3860.7	0.148	363.0	1.2E-02	1.8E-02	0.15	0.05
	4	14050.8	0.168	71.4	1.1E-02	9.10E-02	0.86	0.05

mobile and immobile porosity domains, emphasising that dispersion processes were largely unchanged under the prevailing conditions. The first-order mass transfer coefficient (ω_1) was calculated as 0.05 T^{-1}, suggesting negligible interaction between mobile and immobile porosity, further supporting the hypothesis that the flow primarily occurred within fractures with limited exchange with the surrounding matrix. This analysis highlights the dominant role of advective flow in the fractured quartzite, with minimal influence between flowing and stagnant zones or porosity exchange, consistent across both models. Both models produced similar results, particularly regarding the number of flow channels (N=4), indicating that tracer transport was primarily confined to fractures with limited interaction with no-flow zones. Although Model 2 (MDP-2RNE) incorporates parameters for dual-porosity exchange, the comparable

outcomes suggest that the simpler MDMi model effectively captures the transport dynamics under dry conditions, making it a more efficient and interpretable choice.

The findings indicate that blasting activities likely altered flow patterns, channel connectivity, and preferential flow pathways within the fractured quarry system. The second tracer test, characterised by $N=4$ flow channels, indicated a well-defined flow path, demonstrating the impact of blasting on flow dynamics. This sequence highlights the way in which anthropogenic activities, specifically blasting, can lead to the reconfiguration of flow pathways, thereby influencing the overall hydrodynamics of the system.

While models like MDMi and MDP-2RNE provide mathematically coherent fits, it is crucial to assess their practical applicability in representing hydrogeological processes. The ability to fit a model does not guarantee that it accurately depicts the underlying system. Seasonal variations in flow dynamics influence model complexity. During the wet season, increased rainfall results in higher soil saturation, which generally increases hydraulic conductivity and reduces resistance to flow within fractures. However, the increased saturation may also cause preferential flow paths to shift, necessitating the use of more channels in the model to accurately represent flow interactions across various pathways. In contrast, during the dry season, faster tracer flow rates were observed despite the lower soil saturation. This increase in flow velocities may be due to the greater flushing volume, having temporarily increased the hydraulic head gradient between the injection point and the observation point. This would also be consistent with the lower recovery rate, due to greater flow divergence from the injection point.

Alternatively, this apparent anomaly could also be attributed to the mechanical effects of blasting. Blasting may have widened fracture apertures, allowing for more efficient flow even under low saturation conditions, thus reducing overall resistance and explaining the faster transfer rates observed during dry-season tracer tests. Additionally, differences in flow characteristics between seasons stem from the distinct systems influenced by intermittent blasting activities at the quarry, which alter sediment transport dynamics and fracture morphology.

Overall, these experiments have provided valuable insights into flow rates, fracture pathways, and dispersion characteristics within the altered and fractured environment of the quarry. The results indicate that blasting activities significantly influence these factors, modifying flow rates, directions, and dispersivity. Specifically, blasting activities can create new pathways and alter the physical properties of the fractured rock, leading to changes in subsurface hydrology. With the quarry's closure in November 2023, these findings are especially relevant as they can guide management strategies for decanting and other post-closure plans. The comparative analysis of breakthrough curves and tracer transport parameters enhances the understanding of the hydrogeological characteristics of the site, emphasising the need to consider the impacts of blasting and ongoing operations on groundwater flow dynamics during the closure process.

Conceptual site model

The conceptual site model (CSM) provides a framework for understanding the way in which open-cast mining activities have altered the vadose zone and impacted groundwater flow at the quarry. Mining operations have created fractures and voids in the subsurface, which, once dewatering ceases, fill with water and form pit lakes (Castro and Moore 2000). These changes influence groundwater flow and contaminant transport. The CSM is a simplified representation of the complex subsurface processes, focusing on the behaviour of both environmental and artificial tracers within the fractured rock environment. It emphasises the geological features, including fracture networks and preferential flow paths, that govern water movement and solute transport. The model considers key factors such as tracer sources, transport mechanisms, and their interactions within the system, thereby providing a comprehensive understanding of altered groundwater dynamics.

Environmental tracers such as stable isotopes reveal natural groundwater processes, while artificial tracers such as dye injections provide information on specific flow paths and transport rates. The contact between the diabase intrusions and Daspoort Formation quartzite plays a pivotal role in influencing flow velocity and drainage patterns due to the formation of preferential flow paths along fractures within these geological units. The highly heterogeneous nature of these fractures and their extensive networks control the way in which water moves through the partially saturated vadose zone. This interaction forms the basis of the hydrogeological conceptual model for the site.

Figure 21 illustrates the hydrogeological conceptual model for the quarry, showing the impact of subsurface structures on groundwater flow pathways. The fracture network in the quarry exhibits a classic dual-porosity system, characterised by both fast-moving flow channels and stagnant water zones within the fractures. This system is underpinned by the Daspoort Formation, which consists of quartz arenites rather than quartzites. These sandstones are composed of more than 20% non-quartz minerals, primarily feldspar, which can weather over time and influence the overall porosity and hydraulic conductivity of the formation.

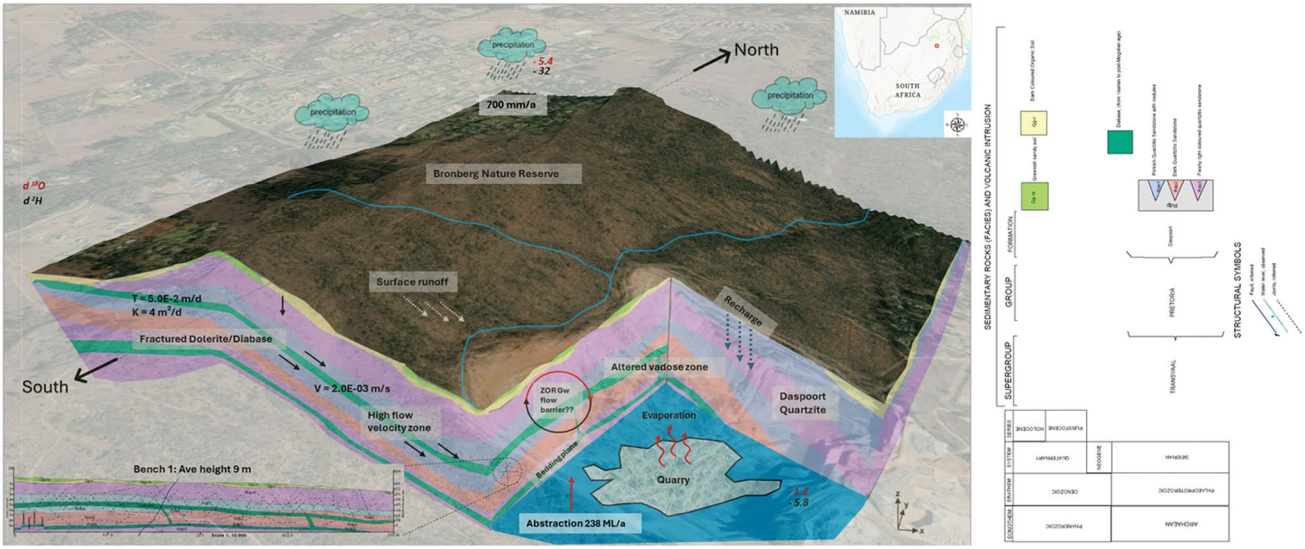

Fig. 21 Hydrogeological conceptual model showing groundwater flow pathways influenced by subsurface structures in an open-pit quarry

The stagnant zones are particularly important in influencing solute transport, often contributing to delayed breakthrough of tracers during wet periods. This behaviour is evident in the hydrogeological responses observed in the field, where intermittent blasting operations in the quarry have substantially altered fracture geometry by promoting sediment deposition or erosion. These modifications impact hydraulic behaviour, leading to changes in flow velocities, turbulence, mixing dynamics, and dispersion characteristics.

The movement of groundwater is heavily dependent on secondary porosity created by fractures, joints, faults, and dykes. These structural features provide critical conduits for groundwater flow, with NW-SE oriented fractures (steeply inclined) promoting flow under normal and strike-slip faulting regimes. These fractures not only serve as conduits for flow but also facilitate drainage towards the quarry pit, where water accumulation occurs.

The three-dimensional geological block model of the quarry site highlights key geological structures, including diabase intrusions, fault planes, and quartzite layers (Fig. S6). The sharp contact between the Daspoort Formation quartzite and the underlying Strubenkop shale, along with the overlying Silverton Formation siltstones and mudstones, is evident. The diabase sill in the quarry has a strike orientation of 45° (northeast-southwest) and dips at 25° towards the southeast, suggesting stable geological conditions during emplacement. Quartzite layers exhibit steep dips (75°) and varying strike orientations (50° and 45° to the northeast), indicating multiple deformation events. The fault plane, with a dip of 80° and a strike of 335°, represents a major tectonic feature that could significantly affect subsurface fluid flow. The near-vertical orientation of this fault suggests potential for substantial vertical displacement, influencing hydraulic conductivity.

In contrast, the sub-horizontal planes in the Daspoort Formation quartzite layers likely promote groundwater movement along preferential pathways, contributing to anisotropic flow conditions. The dip of the diabase sill further influences hydraulic dynamics by creating preferential flow paths, impacting groundwater interaction with surrounding formations. The conceptual model illustrates how these geological structures and subsurface flow pathways interact to govern the hydrogeology of the site, with the fractured network playing a central role in groundwater flow and tracer transport within the altered vadose zone.

Conclusions and recommendations

This study shows that tracer and isotope based techniques, when integrated with structural analysis, offer a powerful means of understanding contaminant transport in an altered vadose zone. The results demonstrate that flow and solute migration are strongly fracture-controlled, shaped by geological structures and intensified by quarry blasting. This highlights the need to consider anthropogenic impacts in conceptualising groundwater systems in similar environments. The application of environmental tracers confirmed active recharge from local rainfall, while artificial tracers revealed variable flow velocities and recovery under different hydrological and operational conditions. These findings point to a dynamic and seasonally responsive system, where fault zones and lithological contacts act as key flow conduits. Beyond characterisation, this work further shows the value of multidisciplinary methods for developing robust,

site-specific conceptual models. Such models are essential for predicting post-closure behaviour, informing risk mitigation, and supporting long-term groundwater management.

It is recommended that future mine closure strategies incorporate tracer studies, isotope monitoring, and structural mapping as standard practice. This will enable adaptive management, early detection of contamination risks, and more effective alignment with environmental sustainability goals.

Future possibilities and limitations

This study has demonstrated the value of combining environmental and artificial tracers with stable isotope analysis to improve understanding of groundwater flow and recharge in an anthropogenically altered vadose zone. While the methods offer a powerful approach for characterising complex flow regimes in fractured media, several limitations remain. The single-season sampling for isotopes provides only a snapshot of recharge conditions, and future research would benefit from multi-seasonal monitoring to capture temporal variability and refine interpretations. Additionally, although the tracer tests captured key flow characteristics, site-specific heterogeneity and mining-induced disturbances present challenges in extrapolating findings beyond the immediate study area. As such, applying these methods in other mined or disturbed environments should be accompanied by detailed hydrogeological characterisation to contextualise results.

Looking ahead, expanding this work through numerical modelling and long-term tracer monitoring would improve predictive capacity and support sustainable mine closure and groundwater management strategies. The approach outlined here provides a transferable framework that can be adapted to similar post-mining environments globally, particularly where fractured vadose zones are influenced by anthropogenic change.

Supplementary Information The online version contains supplementary material available at https://doi.org/10.1007/s12665-025-12318-w.

Author contributions Yazeed van Wyk, Kai Witthüser, Eunice Ubomba-Jaswa contributed to the study conception and design. Methodology execution, data collection and analysis were performed by Yazeed van Wyk, Jacques Bodin, Kai Witthüser, Eunice Ubomba-Jaswa, Mike Butler. The first draft of the manuscript was written by Yazeed van Wyk and all authors contributed and commented on subsequent versions of the manuscript. All authors read and approved the near final version of the manuscript. Matthys Dippenaar managed the research, and finalised the content and formatting of this manuscript for submission to the journal.

Funding Open access funding provided by University of Pretoria.
This work was supported by grant numbers C2020_2021−00581, K5/2499; K5/ 2326; KV 243/10 and TT 584/13. Matthys Dippenaar acquired this research support from the Water Research Commission (WRC) of South Africa (www.wrc.org.za). The authors declare that they have no other funds, grants, or support were received during the preparation of this manuscript.

Data availability No datasets were generated or analysed during the current study.

Declarations

Competing interests The authors declare no competing interests.

References

Bailey AK, Pitman WV (2016) Water Resources of South Africa, 2012 Study (WR2012). Water Research Commission. Pretoria. South Africa

Bănăduc D, Simić V, Cianfaglione K, Barinova S, Afanasyev S, Öktener A, McCall G, Simić S, Curtean-Bănăduc A (2022) Freshwater as a sustainable resource and generator of secondary resources in the 21st century: stressors, threats, risks, management and protection strategies, and conservation approaches. Int J Environ Res Public Health 19(24). https://doi.org/10.3390/ijerph192416570

Barnard HC (2000) An explanation of the 1:500 000 general hydrogeological map: Johannesburg 2526. Department of Water Affairs and Forestry. Pretoria. South Africa

Baudoin M-A, Vogel C, Nortje K, Naik M (2017) Living with drought in South Africa: lessons learnt from the recent El Niño drought period. Int J Disaster Risk Reduct 23:128–137. https://doi.org/10.1016/j.ijdrr.2017.05.005

Bezie G, Chala ET, Jilo NZ, Birhanu S, Berta KK, Assefa SM, Gissila B (2024) Rock slope stability analysis of a limestone quarry in a case study of a National cement factory in Eastern Ethiopia. Sci Rep 14(1):18541

Bodin J (2020) MFIT 1.0.0: Multi-Flow inversion of tracer breakthrough curves in fractured and karst aquifers. Geosci Model Dev 13(6):2905–2924. https://doi.org/10.5194/gmd-13-2905-2020

Bowen GJ, Revenaugh J (2003) Interpolating the isotopic composition of modern meteoric precipitation. Water Resour Res 39(10). https://agupubs.onlinelibrary.wiley.com/doi/full/https://doi.org/10.1029/2003WR002086

Bozan C, Wallis I, Cook PG, Dogramaci S (2022) Groundwater-level recovery following closure of open-pit mines. Hydrogeol J 30(6):1819–1832

Braune E, Xu Y (2010) The role of ground water in sub-Saharan Africa. Groundwater 48(2):229–238. https://doi.org/10.1111/j.1745-6584.2009.00557.x

Candeias C, Ávila P, Coelho P, Teixeira JP (2018) Mining Activities: Health Impacts. Encyclopedia of Environmental Health (Second Edition). (Reference Module in Earth Systems and Environmental Sciences). Elsevier. 415–435. https://doi.org/10.1016/B978-0-12-409548-9.11056-5

Castro JM, Moore JN (2000) Pit lakes: their characteristics and the potential for their remediation. Environ Geol 39:1254–1260. https://doi.org/10.1007/s002549900100

Christensen TH, Kjeldsen P, Bjerg PL, Jensen DL, Christensen JB, Baun A, Heron G (2001) Biogeochemistry of landfill leachate plumes. Appl Geochem 16(7–8):659–718

Clark ID, Fritz P (1997) Environmental Isotopes in Hydrogeology. 1st Edition. CRC Press/Lewis Publishers. Boca Raton, Florida, USA. https://doi.org/10.1201/9781482242911

Cook P, Dogramaci S, McCallum JL, Hedley J (2017) Groundwater age, mixing and flow rates in the vicinity of large open pit mines, Pilbara region, Northwestern Australia. Hydrogeol J 25(1):39–53. https://doi.org/10.1007/s10040-016-1467-y

Craig H (1961) Isotopic variations in meteoric waters. Science 133(3465):1702–1703. https://doi.org/10.1126/science.133.3465.1702

Cuthbert MO, Taylor RG, Favreau G, Todd MC, Shamsudduha M, Villholth KG, MacDonald AM, Scanlon BR, Kotchoni DOV, Vouillamoz J-M et al (2019) Observed controls on resilience of groundwater to climate variability in sub-Saharan Africa. Nature 572:230–234. https://doi.org/10.1038/s41586-019-1441-

Dansgaard W (1964) Stable isotopes in precipitation. Tellus 16(4):436–468. https://doi.org/10.3402/tellusa.v16i4.8993

Dhansay T (2021) Shattered crust: how brittle deformation enables critical zone processes beneath Southern Africa. S Afr J Geol 124(2):519–536

Dhansay T, Navabpour P, De Wit M, Ustaszewski K (2017) Assessing the reactivation potential of pre-existing fractures in the Southern Karoo, South Africa: evaluating the potential for sustainable exploration across its critical zone. J Afr Earth Sc 134:504–515. https://doi.org/10.1016/j.jafrearsci.2017.07.020

Döll P, Jiménez-Cisneros B, Oki T, Arnell NW, Benito G, Cogley JG, Jiang T, Kundzewicz ZW, Mwakalila S, Nishijima A (2015) Integrating risks of climate change into water management. Hydrol Sci J 60(1):4–13. https://doi.org/10.1080/02626667.2014.967250

DWAF (1999) Hydrogeological map series of the Republic of South Africa. Department of Water Affairs and Forestry (DWAF), Pretoria, South Africa

Eriksson PG, Reczko BFF (1995) The sedimentary and tectonic setting of the Transvaal supergroup floor rocks to the bushveld complex. J Afr Earth Sc 21(4):487–504. https://doi.org/10.1016/0899-5362(95)00111-5

Eriksson PG, Schreiber UM, Van der Neut M, Labuschagne H, Van der Schyff W, Potgieter G (1993) Alternative marine and fluvial models for the non-fossiliferous quartzitic sandstones of the early proterozoic daspoort formation, Transvaal sequence of Southern Africa. J Afr Earth Sci (and Middle East) 16(3):355–366. https://doi.org/10.1016/0899-5362(93)90055-U

Eriksson PG, Altermann W, Hartzer FJ (2006) The Transvaal supergroup and its precursors. In: Johnson MR, Anhaeusser CR, Thomas RJ (eds) The geology of South Africa. Geological Society of South Africa, Johannesburg and Council for Geoscience, Pretoria, South Africa, pp 237–260

Fernando WAM, Ilankoon IMSK, Syed TH, Yellishetty M (2018) Challenges and opportunities in the removal of sulphate ions in contaminated mine water: A review. Miner Eng 117:74–90. https://doi.org/10.1016/j.mineng.2017.12.004

Ingrao C, Strippoli R, Lagioia G, Huisingh D (2023) Water scarcity in agriculture: an overview of causes, impacts and approaches for reducing the risks. Heliyon 9(8):e18507

Kendall C, McDonnell JJ (eds) (2012) Isotope tracers in catchment hydrology. Elsevier Science

Khan RA, Khan NA, El Morabet R, Alsubih M, Qadir A, Bokhar A, Manickam S (2022) Geospatial distribution and health risk assessment of groundwater contaminated within the industrial areas: an environmental sustainability perspective. Chemosphere 303:134749

Knüppe K (2011) The challenges facing sustainable and adaptive groundwater management in South Africa. Water SA 37(1). https://doi.org/10.4314/wsa.v37i1.64110

Kotzé Y, van der Merwe J, Gomo M, Molaolwa G, de Lange J, Esterhuizen L, Mantyeane A (2019) Training Manual for Groundwater Resource Management and Groundwater Governance for Municipalities in South Africa. WRC Report No. 2447/1/19. Water Research Commission. Pretoria, South Africa

Li WC, Dai F, Wei YQ, Wang ML, Min H, Lee LM (2016) Implication of subsurface flow on rainfall-induced landslide: a case study. Landslides 13:1109–1123

Linacre ET (1994) Estimating U.S. Class A pan evaporation from few climate data. Water Int 19(1):5–14. https://doi.org/10.1080/02508069408686189

Luo A, Wang G, Dong S, Wang H, Shi Z, Ji Z, Xue J (2022) Effect of large-scale mining drainage on groundwater hydrogeochemical evolution in semi-arid and arid regions. Front Environ Sci 10:926866

Lynch S, Schulze RE (2006) Rainfall database. In: Schulze RE (ed) South African atlas of climatology and agrohydrology. WRC report no. 1489/1/06. Water Research Commission, Pretoria, South Africa

Mahlalela PT, Blamey RC, Hart NCG, Reason CJC (2020) Drought in the Eastern cape region of South Africa and trends in rainfall characteristics. Clim Dyn 55:2743–2759. https://doi.org/10.1007/s00382-020-05413-0

McDonald RI, Weber K, Padowski J, Flörke M, Schneider C, Green PA, Montgomery M (2014) Water on an urban planet: urbanization and the reach of urban water infrastructure. Glob Environ Change 27:96–105. https://doi.org/10.1016/j.gloenvcha.2014.04.022

Mook WG (2000) Environmental isotopes in the hydrological cycle: Principles and applications. IHP-V, Technical Documents in Hydrology 1. Vol. IV, No. 39, UNESCO, Paris

Morris A, Ferrill DA, Henderson DB (1996) Slip-tendency analysis and fault reactivation. Geology. 24(3):275–278.https://doi.org/10.1130/0091-7613(1996)024%3C0275:STAAFR%3E2.3.CO;2

Nordstrom DK, Blowes DW, Ptacek CJ (2015) Hydrogeochemistry and microbiology of mine drainage: an update. Appl Geochem 57:3–16. https://doi.org/10.1016/j.apgeochem.2015.02.008

Northey SA, Mudd GM, Saarivuori E, Wessman-Jääskeläinen H, Haque N (2016) Water footprinting and mining: where are the limitations and opportunities? J Clean Prod 135:1098–1116. https://doi.org/10.1016/j.jclepro.2016.07.024

Parsons R (1995) A South African aquifer system management classification. Prepared for water research commission and department of water affairs and forestry. WRC report no. KV 77/95. Water Research Commission, Pretoria, South Africa

Pegram GGS, Sinclair S, Bárdossy A (2016) New methods of infilling Southern African rain gauge records enhanced by annual, monthly and daily precipitation estimates tagged with uncertainty. WRC report no. 2241/1/15. Water Research Commission, Pretoria, South Africa

Ran Q, Hong Y, Li W, Gao J (2018) A modelling study of rainfall-induced shallow landslide mechanisms under different rainfall characteristics. J Hydrol 563:790–801

Stumm W, Morgan JJ, Drever JI (1996) Aquatic chemistry. J Environ Qual 25(5):1162

Van der Neut M (1990) Afsettingstoestande van die Pretoria Groep gesteentes in die Pretoria-Bronkhorstspruit-Delmas gebied. MSc Thesis. University of Pretoria. Pretoria, South Africa

van Wyk Y, Dippenaar MA, Ubomba-Jaswa E (2024) Enhancing hydrological analysis by incorporating environmental and artificial tracers of an altered vadose zone: A systematic review. J Afr Earth Sc 212:105209. https://doi.org/10.1016/j.jafrearsci.2024.105209

Vegter JR (1995) An explanation of a set of National groundwater maps. WRC report no. TT 74/95. Water Research Commission, Pretoria, South Africa

Vervoort A, Declercq P-Y (2018) Upward surface movement above deep coal mines after closure and flooding of underground workings. Int J Min Sci Technol 28(1):53–59

White JT, Doherty JE, Hughes JD (2014) Quantifying the predictive consequences of model error with linear subspace analysis. Water Resour Res 50(2):1152–1173 Quantifying the predictive consequences of model error with linear subspace analysis

Younger PL, Wolkersdorfer C (2004) Mining impacts on the fresh water environment: technical and managerial guidelines for catchment scale management. Mine Water Environ 23:s2–s80. https://doi.org/10.1007/s10230-004-0028-0

Zeng B, Zhang Z, Yang M (2018) Risk assessment of groundwater with multi-source pollution by a long-term monitoring programme for a large mining area. Int Biodeterior Biodegrad 128:100–108. https://doi.org/10.1016/j.ibiod.2017.01.002